Phenomenological model coupling stress transfer with photon diffusion for interpreting the kinetics of delayed ultraweak photon emission from organism in response to a bolus or step stress

Daqing Piao, PHD
School of Electrical and Computer Engineering, Oklahoma State University, Stillwater, OK, 74078, USA
Department of Veterinary Clinical Sciences, Center for Veterinary Health Sciences, Oklahoma State University, Stillwater, OK 74078, USA
**Correspondence: daqing.piao@okstate.edu*

Abstract:
Much remains to be understood for delayed ultraweak photon emission (UPE) from organism in association with oxidative burst following external perturbation, a phenomenon that has been experimented for over three decades. Delayed UPE often decays hyperbolically; yet, it is not uncommon to have delayed UPE that reveals first-order kinetic patterns characterized by single-exponential, double exponential, or multi-exponential changes. Some delayed UPEs also presented transient patterns that are characteristic of second-order responses. A soliton-based photon-storage model has addressed the hyperbolic decaying pattern of delayed UPE; however, there are questions outstanding regarding modeling other non-hyperbolic kinetics as well as the large range of temporal scales of delayed UPE that can vary from 8.5 microseconds to many hours. This work proposes an alternative, phenomenological model-framework for interpreting the various kinetic patterns of delayed UPE following stress. The delayed UPE is considered to be governed by two sequential phases: a stress-transfer phase that transforms the external stress to photo-genesis for emitting photons, and a photon-diffusion phase that transmits the photons emitted by the photo-genesis to the surface of organism for being detected as delayed UPE. Time-resolved photon diffusion analysis reveals that any delayed UPE in organism with a delay time >100ns cannot be addressed by the inherent temporal spread that realistic tissue scattering will cause. A slow stress-transfer phase is thus required to explain the delay time-scales of delayed UPE at a minimum of 8.5μs as reported experimentally. The stress-transfer phase is hypothesized to carry the following types of responses: single or multiple 1st-order low-pass, single 2nd-order low-pass with various damping factors, and single 2nd-order band-pass with various damping factors. A single 1st–order low-pass response with a time-varying kinetic rate is also analyzed. The responses of these modeled pathways to bolus and step inputs demonstrate that a kinetic pattern other than the exact single-exponential one may have multiple causes.

Keywords: delayed ultraweak photon emission; light propagation in tissues; stress transfer.

1. Introduction

Complex investigative interests have been raised over many decades, regarding the spontaneous steady-state or stress-stimulated varying emission of extremely weak light from an organism. This so-called ultraweak photon emission (UPE) [1] distinguishes itself from other forms of bio-illumination in terms of intensity, spectrum, spatial correlation and temporal pattern [2-4], which collectively suggest under-resolved mechanistic origins. Many terms have appeared historically in referring to UPE phenomena: weak luminescence [5], low-level chemiluminescence [6], spontaneous chemiluminscence [7], biophoton(s) emission [8, 9], ultra-weak bioluminescence [10], autoluminescence [11], spontaneous ultra-weak light emission [12], etc. The situation that many terms have been developed to describe experimental observations suspected of the same underlying principles stories the slowly evolving understanding of UPE that has yet to reach adequate consensus.

The extremely weak illumination level makes UPE difficult to detect and unattractive for application. As a result, much controversy remains regarding the mechanistic, analytical, and practical aspects of UPE. The hypothesized connections of UPE with cognition [13, 14] further complicate the exploration of UPE phenomenon. Regardless of the not-yet-adequately-resolved biological origins and unclear neurophysiological engagements of UPE, the UPE detection is an exact matter of photon-detection that has to be dictated by the principles of physics, including those prescribing photon propagation in medium and at the interface of two media. The detection of UPE involves optimizing the optical, spectral, spatial, and temporal configurations of photo-electronic detection instrument, similar to detecting any other weak illumination wherein increasing the sensitivity and suppressing the noise cross-talk is essential [15]. UPE carries a continuum spectrum covering the visible band and extending to near-infrared band [6, 8, 16-24]. Although the continuum spectral presentation of UPE is still elusive [24], recent studies have identified electron-related energy transitions of multiple types that occur in mitochondrial chemical chain-reaction and result in broad-band photon emissions of multiple peaks that when combined conform to the continuum spectrum of delayed UPE [25]. The continuum spectrum of UPE also allows controlling the spectral bandwidth of detection optics for noise benefit and to probe a specific spectral response [26].

A more interesting aspect of the physical principles shared by UPE detection with other light acquisition scenarios is the “boundary effect” that governs both ballistic and non-ballistic light transmission from one medium to the other. An explicit example of “boundary effect” on UPE detection was demonstrated by Nakamura and Hiramatsu [27] in acquiring biophotons from human hand by using a photomultiplier tube (PMT). When there was an air layer between the palm and the glass window of the PMT, about 100 photon counts per second was obtained. When mineral oil was used to buffer the hand with the glass-window of the PMT, about 200 photon counts per second was obtained. This was approximately twice as much in comparison to the former one. Similar level of enhancement of the photon counts was obtained also by water-immerged contact of the PMT glass window with the palm or direct contact of the PMT glass window with the palm. The enhancement of photon passage from tissue to PMT light collection chamber by removing an air layer between the tissue and the detection glass window of the PMT was the result of a better matching of refractive index across the boundary that the photons must pass, wherever the photons were generated (i.e. the site of photo-genesis) within the tissue. This enhancement of UPE photon is the exact presentation of the boundary-value principle of light transmission between two media. Were UPE photons generated on the surface of the tissue, the transmission of UPE photons from tissue to the outer interfacing layer, be it the PMT glass window or the air between the tissue and the PMT glass window, will be primarily ballistic and so the transmission of photons from the superficial tissue layer to the detector is then affected by the Fresnel refraction. Were UPE photons produced inside the tissue, the arriving of UPE photons originating from wherever the site of photo-genesis within the tissue is to the surface of tissue before coupled to the outer interfacing layer must involve diffuse photon propagation within the tissue due to scattering by cellular and subcellular microstructures and absorption by chromophores, if neglecting any other light-tissue interactions.

Delayed UPE is a phenomenon of the increase of UPE photon count from the baseline spontaneous level following an external stimulation of various types [28, 29]. The increase of UPE intensity in the delayed UPE in comparison to the base-line is attributed to oxidative burst caused by metabolic responses to any external stress or shock that perturbs the homeostasis [30-32]. Delayed UPE in response to photo-illumination has shown the shortest delay time recorded, a minimum of 8.5μs after tuning off the photo-illumination [33], and the intensity of its initial peak can be several orders of magnitude stronger than the spontaneous steady-state UPE [34, 35]. Other types of external stimulation, such as chemical [28], mechanical [3], thermal/environmental [36], radiative [37], electrical [38], and magnetic [39] have shown to induce delayed UPE of relatively smaller change over the baseline level than the photo-stimulation. Delayed UPE in response to non-photic stimulation is usually much slower for being detected and can last long (up to several hours) after the stress or shock was removed. Because delayed UPE responds to external stress through metabolic pathway that results in oxidative burst, controlling external stress thus can modulate the delayed UPE and suggestions have been made to use the kinetics of delayed UPE to probe the oxidative stress pathway [35, 40]. This viable application of delayed UPE with potential in physiological health is a challenge in the present, because the weak level of photon emission of delayed UPE requires long acquisition time and highly sensitive photon-counting devices. Exploring the application of delayed UPE is also difficult in the present, because much remains to be associated between the various kinetic patterns of delayed UPE and the external stress or shock that triggers the delayed UPE.

Delayed UPE in response to photo-illumination is generally reported to decay hyperbolically [41, 42]. A hyperbolic decay pattern of delayed UPE is projected to indicate coherence of UPE photo-genesis [28, 43] of which the underlying mechanism is not resolved. It is worth noting that, there are many presentations of delayed UPE kinetics that do not fit to a hyperbolic pattern. Single-exponential kinetic patterns are found commonly in delayed UPE phenomena (many are from plants) that are much slower than those associated with photo-illumination [44-47]. Double-exponential kinetic patterns are also appreciable in delayed UPE of organisms experiencing photic [48], mechanical [3, 45, 49, 50], chemical [51-58], and radiative [37] stresses. Some of these delayed UPE phenomena have the photons recorded continuously from several seconds to hours after the removal of the external stress. In quantitating these decay kinetics, models of correlated coherent many-solitons existing in organism [42, 59] were developed after a coherent-state approach initially proposed by Popp [43, 60]. The soliton-based models have been successful for interpreting the hyperbolic decay pattern of delayed UPE when stimulated by ultraviolet light, and justifying the non-linear dependence of the delayed UPE yield on the intensity of photo-illumination only [61, 62]. However, there are delayed UPEs following photo-illumination that seem to present multi-exponential kinetics [34] rather than a simple hyperbolic change. Some delayed UPE phenomena clearly have revealed single exponential kinetics [47], occasionally mixed with double-exponential patterns [38]. There are also delayed UPE phenomena that reveal transient kinetic patterns of rapid oscillation overlapping on a much slower global profile and bi-phasic patterns in response to a temporally monotonic stimulation [55, 56, 63]. Those rapid oscillatory patterns and biphasic patterns in response to simple temporarily monotonic stimulation cannot be justified by a first-order response but are straightforward to be seen as a second-order response. Besides the kinetic varieties of delayed UPE, the broad temporal scales of delayed UPE covering 10s of microseconds to several hours in responding to various stress types may also be difficult to project with a model that addresses the hyperbolic decay pattern alone.

This work proposes an alternative, heuristic modeling framework for interpreting the various kinetic patterns of delayed UPE following bolus and step stresses that form the basis for the analysis of more complicated stress patterns. The temporal profiles of delayed UPE is considered to be governed by two sequential phases: a stress-transfer phase that transforms the external stress to photo-genesis that produces photons, and a photon-diffusion phase that diffusely transmits the photons produced by the photo-genesis to the surface of organism for being detected as the delayed UPE. Wherever the site of

photo-genesis is, any photons originating in tissue that reach the surface to be detected as the delayed UPE will experience tissue scattering and absorption. Therefore the photon-paths from the site of photo-genesis to the surface site will be modulated by tissue scattering and that tissue-scattering will cause temporal spread or broadening of the photons in comparison to the ballistic transmission between the site of photo-genesis to the surface site of detection. In order to identify the temporal causes of the delayed UPE, it is imperative to know how much temporal spread or broadening can be resulted from tissue scattering alone on the photons that are detected at the surface as delayed UPE. Analysis of time-resolved photon diffusion in an extremely scattering tissue over a domain as large as the cross-section of human (40cm in diameter) reveals that scattering-caused temporal spread or broadening of the photon pack when detected at the organism surface will be narrower than 100ns. Therefore any delayed UPE with a delay time much longer than 100ns has to have a much slower process of photo-genesis to account for the delay observed. The delayed UPE with a minimal delay time of 8.5μs as reported is thus projected to be caused by a slow stress-transfer phase that is coupled to the photon diffusion process to produce the temporal profiles of delayed UPE photons detected at the organism/tissue surface. Theory of linear-time-invariant system is then applied to the stress-transfer phase for modeling the temporal response of the hypothesized stress-transfer pathway to a bolus input and a step input to form the basis of analyzing the response to stress with arbitrary profiles. The hypothesized stress-transfer phase is modeled to be one of the following types of system having constant kinetic rates: single first-order low-pass, dual in-parallel first-order low-pass, three or more in-parallel first-order low-pass, single second-order low-pass with various damping factors, and single second-order band-pass with various damping factors. A single first-order low-pass transfer pathway with a time-varying kinetic rate is also implemented. The responses of these hypothesized pathways to bolus and step inputs are compared numerically to illustrate the appearances of single-exponential, double-exponential, hyperbolic, and oscillatory decay patterns in association with different system and input conditions.

The rest of the paper is organized as the following: Section 2 tabulates approximately 66 reports of delayed UPE, according to the type of stimulation and the kinetic pattern in response to the external stimulation. This survey illustrates the variety of kinetics of delayed UPE, and some common patterns of the kinetic responses to a specific type of external stress. Section 3 develops the time-resolved photon diffusion in a large spherical diffusive tissue domain as the exaggeration for a large organism in order to discover the upper limit of the temporal spread of photon diffusion that can be caused by tissue scattering. Section 3 concludes that the delayed UPE with a minimal delay time of 8.5μs as surveyed in Section 2 cannot be addressed by the temporal spread associated with tissue scattering that UPE photons must experience when propagating from a site of photo-genesis to the surface site of detection. Section 4 presents the models involving linear time-invariant system hypothesized for the stress-transfer pathway needed to produce photons at the site of photo-genesis at a temporal pace much slower than the photon diffusion process that transmits the photons in tissue to the surface site of detection. The temporal responses of each individual system representing a possible stress-transfer pathway to bolus and step inputs are developed. Section 5 numerically compares the responses of the multiple hypothesized stress-transfer pathways to a bolus input and a step input as modeled in Section 4. Unique patterns of transfer responses are identified. Some transfer responses are found difficult to be distinguished from others without further knowledge of the kinetic pathway. Section 6 discusses the potential of utilizing unique kinetic patterns for probing stress-transfer pathways and using frequency-spectrum analysis to discriminate among stress-transfer responses of similar patterns.

2. Survey of the kinetics of delayed UPE

Delayed UPE from organism was reported as early as 1983 from isolated perfused rat heart [58] and in 1987 from enzymes exposed to chemical stress [57]. These reports were followed up by more than 60 studies in the subsequent 3 decades as are summarized in this section. The delayed emission of ultra-weak photons has shown to associate

with various types of external stimulation or stress that was applied instantaneously, continuously, or intermittently. These stress types that have been reported can be categorized as photic, chemical, mechanical, thermal/environmental, radiative, electrical, and magnetic. These reports of delayed UPE generally presented an enhancement of the UPE emission immediately after the removal of the stress before decaying to the baseline-level of the spontaneous steady-state UPE. This section tabulates the kinetics of delayed UPE of approximately 66 reports, for the purpose of identifying the types of decay patterns and the range of temporal scales presented by delayed UPE observed in a variety of organisms and stress types. This survey is imperative, because the kinetic varieties of delayed UPE have not been collectively presented and the varieties of kinetic patterns of delayed UPE indicate the complexities linking the stress to the response. The possibility of multiple stress-response paths or kinetic patterns must be appreciated when the underlying mechanisms are to be probed. This survey is informative, since the temporal scales of delayed UPE will discern if it is possible for a photon to remain in the tissue by way of physically mandated mechanisms such as tissue scattering after the photon is generated, over the entire length of the delay time measured at the organism surface to become the delayed UPE, after the removal of a stress.

Most reports of delayed UPE which are tabulated in **Table 1** are observed with decay of the delayed UPE photon count in response to the removal of an external stress. Many delayed UPE in response to photic-stress presented the decay of the delayed UPE from a level that is several orders of magnitude greater than the baseline level. The decay of the delayed UPE from a level greater than the baseline must have been preceded by a phase wherein the UPE intensity increased from the baseline to the level at which the delayed UPE was started to be measured. Even though some had reported rising phases of the delayed UPE in response to the onset of a specific stimulation, it is the decaying phase of the delayed UPE in each of these reports that has sometimes been fitted with or interpreted by using either single exponential, double exponential, four or seven exponential or hyperbolic functions. This survey thus groups the delayed UPE according to the decaying pattern, i.e., the rate of temporal reduction of the delayed photon count $\boldsymbol{q(t)}$ as a function of the time-delay $\boldsymbol{t}$ that is counted from the removal of the stimulation, as one of the following three types of decays:

(1) The decay kinetics that is fitted by or can be interpreted with a single exponential function of

$$\boldsymbol{q(t) = A_1 \cdot exp(-k_1 t)} \text{ or } \mathbf{q(t) = A_1 \cdot exp(-t/\tau_1)} \quad (1)$$

where $\boldsymbol{A_1}$ is photon count, $\boldsymbol{k_1}$ is decay rate (1/second) and $\boldsymbol{\tau_1}$ is time constant (second).

(2) The decay kinetics that is fitted by or can be quantitated better with two or more exponential functions configures as

$$\boldsymbol{q(t) = \sum_{m=1}^{M} A_m \cdot exp(-k_m t)} \text{ or } \boldsymbol{q(t) = \sum_{m=1}^{M} A_m \cdot exp(-t/\tau_m)} \quad (2)$$

where $\boldsymbol{M \geq 2}$, $\boldsymbol{A_m}$ is photon count, $\boldsymbol{k_m}$ is decay rate (1/second) and $\boldsymbol{\tau_m}$ is time constant (second), all corresponding to the m-th exponential component.

(3) The decay kinetics that is fitted by or can be interpreted the best with a hyperbolic function of

$$\boldsymbol{q(t) = A_h(B_h + k_h t)^{-\alpha_h}} \text{ or } \boldsymbol{q(t) = A_h(B_h + t/\tau_h)^{-\alpha_h}} \quad (3)$$

where $\boldsymbol{A_h}$ is a photon count, $\boldsymbol{B_h}$ is a dimensionless term, $\boldsymbol{k_h}$ is decay rate (1/second), $\boldsymbol{\tau_h}$ is time constant (second), and $\boldsymbol{\alpha}$ denotes the decay power (dimensionless). These three types of decay patterns are plotted in **Figure 1** after normalizing each to its respective peak amplitude to differentiate the early decay behavior and the latter decay pattern among the three. In surveying the reports of delayed UPE in Table 1, the decay patterns that were presented with original analytical fittings are organized according to Eqs. (1-3) and the parameters specified when available. For other reports wherein the fitting of the decay kinetics is not given, a kinetic (decay) time scale is estimated from the decay patterns plotted according to the following principles: (1) If the decay is reported with a linear scale of the photon count as the ordinate, the time that it takes to drop to 1/2 of the initial value of the photon count is estimated from the ordinate of the plot and assigned as the 1/2 life-time; (2) If the decay is reported with a logarithmic scale of the photon count as the ordinate, the time that it takes to drop to $1/10^{th}$ of the initial value of the photon count is estimated from the ordinate of the plot and assigned as the $1/10^{th}$ life-time. Either the ½ life time or the $1/10^{th}$ life-time will inform how fast the initial decay of the delayed UPE, by comparing to the total duration of observing the kinetic changes of delayed UPE. There are also several reports revealing fast oscillations as well as bi-phasic changes of delayed UPE that individually or collectively infer the existence of non-first-order patterns or second-

order pattern as the first approximation. For these reports, the three cells with the table corresponding to the three patterns of decay specified by Eqs. (1-3) are merged to one cell in order to visualize the differences of these 2nd-order like patterns from other decay patterns that are essentially 1st -order ones.

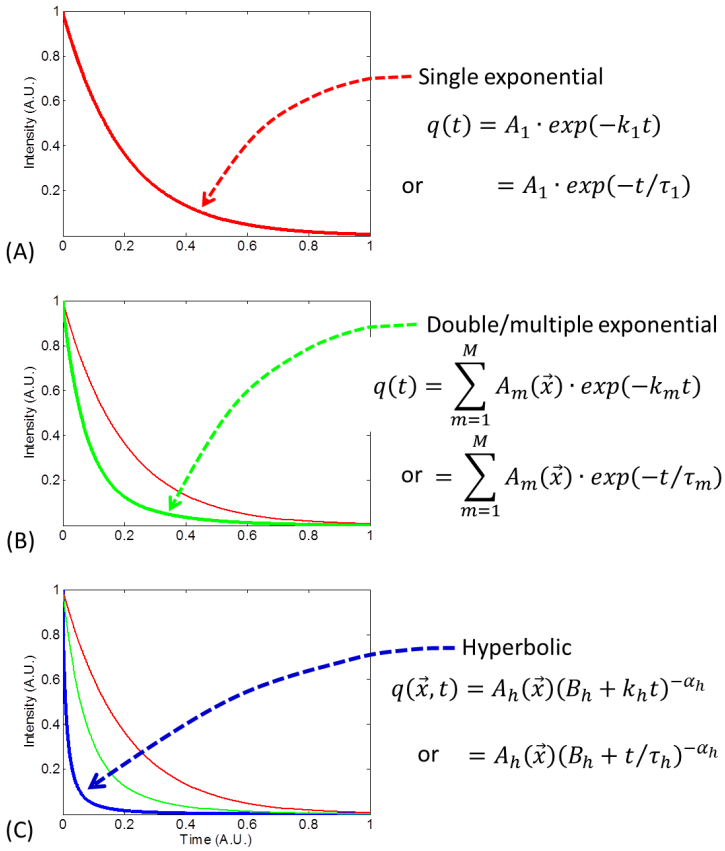

Figure 1. Patterns that have been used in describing the decaying kinetics of delayed UPE. All curves are normalized with respect to the value at a time of origin. (A) Single exponential decay that is defined by one time constant; (B) double or multiple exponential decay that is characterized by two or more time constants. (C) Hyperbolic decay that is shaped by a time-constant as well as a power factor.

Table 1 leads to the following summative information for the approximately 66 reports of delayed UPE that are surveyed: (1) the types of the stimulation reported to induce delayed UPE include photic (21 cases, 31.3%), chemical (33 cases, 47.8%), mechanical (6 cases, 9.0%), thermal/environmental (3 cases, 4.5%), radiative (2 cases), electrical (1 case), and magnetic (1 case). (2) The shortest delay time of delayed UPE was 8.5$\boldsymbol{\mu s}$ that was acquired from mouse melanoma cells in response to the removal of ultraviolet illumination [33]. The delayed UPE from organisms after exposing to stimulation that is not photic is generally much slower than that from organisms exposed to photic stimulation. (3) The temporal spread of the delayed UPE can extend to several and even a hundred hours. (4) The delayed UPE that has presented faster decay kinetics generally had greater initial level of intensity of the delayed UPE than those that decayed slowly. In terms of how the delayed UPE reduces over time after removal of the corresponding stress or stimulation, only 34.8% (23 cases) clearly have presented hyperbolic patterns, whereas 25.8% (17 cases) have revealed decay kinetics that were either fitted by or better interpreted with double or multiple exponential patterns, and as many as 47.0% (31 cases) of the delayed UPE phenomena can be appreciated as conforming to single exponential decay kinetics. Besides these delay UPE patterns that presented monotonic decay kinetics indicating 1st-order responses, 22.7% (15 cases) have reported kinetic patterns that have either slow bi-phasic pattern or fast oscillation overlapping on a slow global pattern, which can be understood conveniently as 2nd-order responses.

Table 1 Delayed UPE according to the type of external stimulation and the kinetic patterns of decaying of the UPE after stimulation

Stress and subject			**Kinetic patterns and parameters Frist-order kinetics (second order kinetics—merged cells)**			**Kinetic rate or temporal scale**		
Stress type	**Specific stress**	**Organism and additional condition**	**Single exp.** 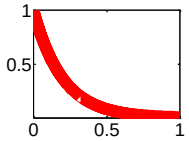 $A_1 \cdot e^{-k_1 t}$	**Double/multiple exp.** 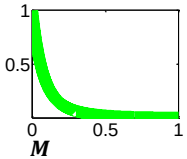 $\sum_{m=1}^{M} A_m \cdot e^{-k_m t}$	**Hyperbolic** 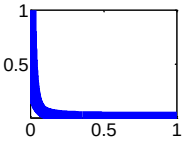 $A_h(B_h + k_h t)^{-\alpha_h}$	**Estimated initial 1/2 lifetime**	**Estimated initial 1/10th life-time** or $\tau_1 = k_1^{-1}$ or $\tau_1 = k_h^{-1}$	**Duration of acquisition of delayed UPE**
Photic	Niggli et al [33] (2005) Wavelength: 337.1nm Pulse width: 5ns Energy: 100±3μJ/pulse	Cloudman S91 mouse melanoma cells			$A_h = 7.1274$ $B_h = 1.0 * 10^{-6}$ $k_h = 1$ $\alpha_h = 1.246$ $A_h = 4.4772$ $B_h = 0$ $k_h = 1$ $\alpha_h = 0.9578$ $A_h = 11.343$ $B_h = 0$ $k_h = 1$ $\alpha_h = 1.0909$		90μs	8.5μs to 100ms
	Musumeci et al [64] (2005) Wavelength: 337nm Pulse width: 5ns Energy: 100±5μJ/pulse	Human fibroblast and melanoma cells			$\alpha_h = [1.5, 1.75]$		800μs [64]	10μs to 100ms
	Baran et al [34] (2013) Wavelength: 337nm Pulse width: 5ns Energy: 100±5μJ/pulse	Human leukemia Jurkat T cell lymphoblasts (mitochondria)		M=[2, 7] $\tau_1 < 10\mu s$ $\tau_m = 22.9\mu s - 8.5ms$ M=7 $\tau_1 < 10\mu s$				10μs to 20ms

				$\tau_m = 13.3\mu s - 8.25ms$				
	Scordino et al [35] (2014) Wavelength: 337nm Pulse width: 5ns Energy: 100µJ/pulse	Follicular (FTC-133) and anaplastic (8305C) human thyroid cancer cell lines, wo/w Berberine hydrochloride treatment			X	60µs		$10\mu s$ —10ms
	Grasso et al [65] (2017) Wavelength: 337nm Pulse width: 0.5ns Energy: 100±5nJ/pulse	Non-tumorigenic breast epithelial MCF10A cell line, after proton irradiation (0.5, 2, 6, 9 Gy)			X	60µs		$10\mu s$ —10ms
	Sun et al [66] (2016) Halogen source	Chinese herb powder		A_1=94100-103115 A_2=10388-15185 τ_1 =509-623 (ms) τ_2 =1398-1688 (ms)				5 minutes
	Grasso et al [67] 2016, PLOS Wavelength: 337nm Pulse width: 5ns Energy: 100µJ/pulse	Mung beans (*Vigna radiata*) seeds			X		1ms	100ms
	Wang et al [68] (2016) Xenon flash lamp	Serum, wo/w narcotics			$(1+\frac{t}{m\tau})^{-m}$	19.3—38.4ms		80ms
	Kim et al [69] (2005) White blue spectrum 30 seconds	Human cancer cells			$A\left(1+\frac{t}{t_0}\right)^{-\alpha}$ A= 106-138 counts/10 ms, $t0$= 3.3-6.4 ms, and α= 0.80-1.17.	300ms		10 seconds
	Chen et al [70] (2012) Xenon flash lamp 5us	Normal and leukemic human sera			$(1+\frac{t}{m})^{-m}$ 111.92ms, 1.276 315.04ms, 1.574			1 second

	Gu and Popp [71] (1992) White light	Rye grain		X	X	3 seconds		10 seconds or longer
	Khabiri et al [72] and Hagens et al [73] (2008) UAV xenon lamp	Skin			X	3~4 seconds		200 seconds
	Slawinski et al [28] (1992) Halogen light (***)	Yeast cells.			x	10 seconds		30 seconds to 120 minutes
	Bajpai and Baipai [74] (1992) Mass dependence	Plant tissue Germinating seeds of Phaseolus aures	X in the first minute	X $0.16C \cdot exp^{-0.065t} + C \cdot exp^{-0.017t}$		80 seconds		200 seconds
	Sauermann et al [45] (1999) Mercury lamp 12.5J/25cm2	Human Skin	X			Minutes		10 minutes
	Kataoka et al [75] (2001) Xenon light (10W/cm2)	Neural tissue	X			Minutes		20 minutes
	Popp et al [76] (1988) White blue light	Living cell population			$A\left(1+\frac{1}{t_0}t\right)^{-k}$	Minutes		28 minutes
	Winkler et al [49] (2009)	Seeds of Cucurbita pepo var. styriacae		XX	X	10s seconds		2500 seconds
	Wang et al [77] (2011) Visible light	Rat eyes			x	10s seconds		1200 seconds
	Prasad and Pospisil [78] (2012) Visible light	Skin chromophore	X	x	x	Minutes		55 minutes
	Bertogna et al [48] (2016)	E coli	(2^{nd} order response)					24 hours
Chemical	Slawinski et al [28] (1992) (***)	Yeast cells Saccharomyces cerevisiae		X	X	Seconds and minutes		30 seconds to 120 minutes
	Kruk et al. [79] (2011)		Pattern unclear, like a single exp			Seconds		70 seconds
	Xie [80] and Chi [81] (2009)	Maze		M=2, 3, or 4		Seconds		49 seconds

	NaCl							
	Maccarrone et al [82] (1997) (***) Water	Cereal	X		XX	Minutes		29 minutes
	Khabiri et al [72] (2008) Hydroperoxide	Skin, bovine serum		X		Seconds		200 seconds
	Hossu et al [83] (2013) Ag nanoparticle	PCa cell	X	X				500 seconds
	Tada and Okazaki [84] (2006) (**) Aequorin	HASMC cell line			X	10s seconds		300 seconds
	Shanei, A. [52] 2017 Hydroperoxide	HT-29 cells	Like a critically damped response			10s seconds		900 seconds
	Popp et al [76] (1988) Poison	Living cell (larvae)	X		X	10s seconds		100 seconds
	Barsacchi et al [58] (1983) Hydroperoxide	Rat heart	(2^{nd} order pattern)			Minutes		60 minutes
	Slawinska and Slawinski [57] (1987) Hydroperoxide and catakase	Synthetic eumelanin and pheomelanin	(2^{nd} order pattern)			Minutes		32 minutes
	Slawinska and Slawinski [55] (1997)	Cereal	(2^{nd} order, oscillation)					4 minutes
	Kimura et al. [56] (1992) (***)	Chinese hamster	(2^{nd} order, oscillation)					70 minutes
	Devaraj et al. [85] (1991)	Rat liver	X	X (2^{nd}-order pattern)				330 minutes
	Hossu et al [53] (2010) Silver nanoparticle	Potato	X (2^{nd} order pattern)					24 minutes
	Kageyama et al [54] (2006)	Rice cell	X, (2^{nd} order pattern)					6 hours
	Shanei et al [52] (2017)	HT-29 cells	(2^{nd} order pattern)					900 seconds

	Hydroperoxide						
	Barshacchi et al [58] (1983) Hydroperoxide	Rat heart	(2^{nd} order pattern)				60 minutes
	Inaba [46] (1988) Toc, DABCO	Living Biological cell liver	X Up and down			10s minutes		80 minutes
	Hideg [86] (1993) (**)	Plants	X			<1 minute		16 minutes
	Kataoka et al [44] (2001) Oxidation	Neural tissue	X			<1 minute		6 minutes
	Slawinski [87] (2003)	Stressing and dying organism	1^{st} order Step-pulse			10s seconds		2000 seconds
	Vladimirov et al [88] (2007) Oxidation	Cytochrome c	X various					550 seconds
	Maccarrone et al [82] (1997)	Human Erytgrikeukemia cells	X Up and down			<1 minute		30 minutes
	Prasad and Pospisil [89] (2011)	Huma skin	X				minute	30 minutes
	Tang and Dai [90] (2014) Glutamate	Neuron	X Multiple steps					500 minutes
	Yoshinaga et al[91] (2006)	Plants	X (2^{nd} order pattern)					14 hours
	Rac et al [32] (2015)	Myeloma cell	X, critically damped up and down			<1 minute		30 minutes
	Prasad et al [92] (2018)	Skin	X (long)			Minutes		30 minutes
	Jaskowska et al [93] (2001) (*****)	Characeae cells	X	XX A_1 =39181/4760 A_2 =4760 τ_1 =12.5min τ_2 =106.3min				3 hours
	Tilbury [94] (1992)	Microorganism	X Up and down			10s minutes		72 hours
	Aoshima et al [95] (2003)	Enzyme	X	X		10s minutes		13 hours
	Bajpai et al [50]	Germinating seeds		X		0.5 minutes		9 minutes

Mechanical	(1991)							
	Oros and Alves [3] (2018)	Leaf	X (1st 250 s)	XX (2nd-order pattern)	X	Minutes		2 hours
	Volodyaev and Beloussov [51] (2015)	Embryo of Xenopus Larvie, cultures of C. utilis	(2nd order pattern)		X	Minutes		Hours
	Winkler et al [49] (2009)	Plants		XX	X	10s seconds		2500 seconds
	Chen et al [96] (2006)	Green soybean	X			10s seconds		20 minutes
	Sauermann et al [45] (1999)	Human skin		X			10 seconds	100 seconds
Temperature/ Environmental	Kobayashi et al [36] (2014)	Azuki bean seeds	X (1st-order)			Minutes		7 hours
	Footitt et al [47] (2016)	Seeds	X	X (2nd-order pattern)		Minutes		100 minutes
	Baipaj and Baipai [50] (1991) Drying	Plant tissues	X rising, falling			Minutes		55 minutes
Radio-active	Goraczko and Slawinski [37] (2004)	Human acid	X X (2nd-order pattern)					100 minutes
	Volodyaev and Beloussov [51] (2015)	Xenopus laevis	X			10s minutes		110 hours
Electrical	Maccarrone et al [38] (1998)	Human K562 cells		XX A_1=5106 A_2=1400 B=186 τ_1=5.5s τ_2==29.5s				150 seconds
Magnetic	Bereta et al [39] (2016)	Yeast cells	X	X		Minutes		16 hours
Total	**66**		**31 (47.0%)**	**17 (25.8%)**	**23 (34.8%)**			

2nd order (15) 22.7%.

3. Temporal spread of the light of UPE spectral relevancy in biological tissue due to photon diffusion

The survey in the previous section has revealed that, the shortest delay-time of delayed UPE was 8.5μs that was associated with photic-stimulation; whereas the longest delay-time of delayed UPE was at the order of hours in response to non-photic stress. An 8.5μs delay of continuous light presence in tissue of a refractive index of 1.4 corresponds to a total photon pathlength of 1.82×10^3 meters---a dimension that is 3 orders of magnitude greater than the height of an adult human. Even scaling the shortest UPE delay one order smaller to compensate the possible after-glow of the photo-stimulation instrument when turned off, a 0.85μs delay of continuous light presence in tissue still means a total photon pathlength of 1.82×10^2 meters in the tissue---which is at least 1000 times greater than the size of many organisms from which the delayed UPE were acquired. Unless there are mechanisms that delay the generation of the photons (e.g. the initiation of the presence of photons in tissue) emitted as delayed UPE after turning off each specific external stress, it would be difficult to imagine that the observed large range of the delay time of delayed UPE is caused entirely by the large path-length (or equivalently the long life-time) of the UPE photons in the tissue after being generated. UPE photon is in the VIS-NIR spectral range that is relatively transparent to biological tissue. When a photon of VIS-NIR spectral band with low intensity appears in the tissue by either external injection or local production, the photon will have to propagate in tissue and experience scattering and absorbing events that collectively will attenuate the light intensity and diffuse the photon path. For time-resolved UPE photon propagation or tissue transmission of the UPE photon originating from a photon source that has a finite lifetime, the tissue scattering will also broaden the UPE temporal profile because of the mixing of ballistic photons with photons that have experienced different amount of scattering events. It is therefore intuitive to compare the maximal temporal spread of photons that can be accounted for by tissue scattering when responding to an instantaneous photon production, against the shortest temporal delay of UPE that has been experimentally observed. This comparison will help identify if a photo-genetic mechanism preceding and much longer in lifetime than the life-time of photon propagation in tissue is imperative to interpreting the very wide range of the temporal delays of delayed UPE measured on the tissue surface.

The greater the scattering tissue domain is, the broader the temporal spread of the photon prorogation becomes. To assess the maximal temporal delay of photons due to scattering, it is thus necessary to assume a large tissue domain and a strong tissue scattering. The light propagation in bulk tissue is accurately described by the radiative transfer equation [97]. In assessing the maximal temporal spread of photon propagation by tissue scattering, the photon diffusion approximation [98] to the radiative transfer equation will be implemented as that accurately describes diffuse photon propagation in scattering biological tissues over a distance substantially longer than the mean scattering pathlength of the photon in tissue. In the following section, the time-resolved diffusion of light of UPE spectral relevancy (i.e., in the VIS/NIR band of biological window to which the photon diffusion analysis is conventional) is treated with spherical Eigen function approach for solving the problem in a spherical tissue geometry. The spherical tissue geometry is used to approximate the tissue domain for delayed UPE detection on the surface because the photons could originate deeply within the tissue, for which case the commonly used semi-infinite tissue-geometry associated with detecting photons diffuse through the tissue after injecting into the tissue at the tissue surface is not as accurate as the spherical geometry. In treating the spherical tissue geometry, a boundary condition for photon diffusion is also implemented to address non-invasive photon acquisition from the tissue surface. The tissue is also assumed to be optically homogeneous for simplicity. The solution of the temporal spread of photon propagation in response to a spatially and temporally impulsive photon source is derived for the spherical tissue domain whose size is orders of magnitude greater than the photon scattering pathlength. The solution is then numerically evaluated for tissue domain with significantly exaggerated scattering conditions comparing to what is realistic for a tissue, in order to assess the maximal temporal spread of photon diffusion measured at the tissue surface that can be caused by tissue scattering.

3.1 Temporal spread of light of UPE spectral relevancy due to tissue scattering in a spherical tissue domain

The equation of time-resolved diffusion of a light of UPE spectral relevancy (in the VIS-NIR spectral band) in a highly scattering biological tissue at a specific wavelength is as the following [99]:

$$\nabla^2\hat{\Phi}(\vec{\chi},t)-\frac{\mu_a(\vec{\chi})}{D(\vec{\chi})}\hat{\Phi}(\vec{\chi},t)-\frac{1}{D(\vec{\chi})\cdot c}\frac{\partial\hat{\Phi}(\vec{\chi},t)}{\partial t}=-\frac{1}{D(\vec{\chi})}\hat{q}(\vec{\chi},t) \quad (4)$$

Where $\hat{\Phi}(\vec{\chi},t)$ is the photon fluence rate (unit: $mm^{-2}\cdot sr^{-1}$) at a spatial position $\vec{\chi}$ and a temporal point t, $\mu_a(\vec{\chi})$ is the absorption coefficient (unit: mm^{-1}), $D(\vec{\chi})=\{3[\mu_a(\vec{\chi})+\mu_s'(\vec{\chi})]\}^{-1}$ is the diffusion coefficient (unit: mm) with $\mu_s'(\vec{\chi})$ being the reduced scattering coefficient (unit: mm^{-1}), c is the speed of light (unit: $mm\cdot s^{-1}$) in the medium, and $\hat{q}(\vec{\chi},t)$ is the source or the photon density (unit: $mm^{-3}\cdot sr^{-1}$). For a homogeneous and boundless medium, the equation of the Green's function of (4) becomes the following:

$$\nabla^2\hat{\Phi}_{inf}(\vec{\chi}',t'|\vec{\chi},t)-\frac{\mu_a}{D}\hat{\Phi}_{inf}(\vec{\chi}',t'|\vec{\chi},t)-\frac{1}{Dc}\frac{\partial\hat{\Phi}_{inf}(\vec{\chi}',t'|\vec{\chi},t)}{\partial t}=-\frac{1}{D}\cdot\delta(\vec{\chi}-\vec{\chi}')\cdot\delta(t-t') \quad (5)$$

where the subscript "inf" represents "infinite geometry". The $\hat{\Phi}_{inf}(\vec{\chi}',t'|\vec{\chi},t)$ of Eq. (5) corresponds to the photon fluence rate at a spatial position of $\vec{\chi}$ and a temporal position of t, in response to an impulsive source stimulation of unity intensity that occurs at a spatial position $\vec{\chi}'$ and a temporal point t'. The temporal profile of $\hat{\Phi}_{inf}(\vec{\chi}',t'|\vec{\chi},t)$ is thus the temporal impulse response of the tissue medium, which when convolved with the temporal profile of any source produces the temporal response of the medium to that actual source.

Since photon diffusion through the biological system has to be causal, we must have $\hat{\Phi}(\vec{\chi}',t'|\vec{\chi},t)=0$ for $t<t'$ for a previously source-less medium. For a medium that has a steady-state baseline emission of photons, any change of the photon emission from the steady-state baseline has to be causal as well. We thus use $\hat{\Phi}(\vec{\chi}',0|\vec{\chi},t)$ to represent the photon fluence rate at a time $t\geq 0$ in response to a source injected (or appearing) at $t'=0$, by normalizing the initial condition to $\hat{\Phi}(\vec{\chi}',0|\vec{\chi},t)\big|_{t=0}=0$.

The Laplace Transform (LT) of Eq. (5) with respect to t when $t'=0$ leads to the following:

$$\nabla^2\hat{\Phi}_{inf}(\vec{\chi}',0|\vec{\chi},s)-\frac{s+\mu_a c}{Dc}\hat{\Phi}_{inf}(\vec{\chi}',0|\vec{\chi},s)=-\frac{1}{D}\cdot\delta(\vec{\chi}-\vec{\chi}') \quad (6)$$

and the solution of which, $\hat{\Phi}_{inf}(\vec{\chi}',0|\vec{\chi},s)$ is the "free-space" solution in the frequency-domain as associated with a source-detector pair in a homogeneous medium of infinite geometry. The solution to Eq. (6) when expressed by using the spherical harmonics is [100]:

$$\hat{\Phi}_{inf}(\vec{\chi}',0|\vec{\chi},s)=\frac{1}{D}(\hat{\mu}_{eff}^s)\sum_{l=0}^{\infty}[i_l(\hat{\mu}_{eff}^s r_<)\cdot k_l(\hat{\mu}_{eff}^s r_>)]\sum_{m=-l}^{l}[Y_{lm}^*(\theta',\phi')\cdot Y_{lm}(\theta,\phi)] \quad (7)$$

where i_l and k_l are respectively the l-th order modified spherical Bessel function of the first and the second kinds, $r_<$ and $r_>$ are respectively the smaller and greater radial coordinates of the source and detector or field position, Y_{lm} is the spherical harmonics function, and $\hat{\mu}_{eff}^s$ is defined as:

$$\hat{\mu}_{eff}^s=\sqrt{\frac{\mu_a}{D}+\frac{s}{Dc}}=\sqrt{s+\mu_a c}\frac{1}{\sqrt{Dc}} \quad (8)$$

Note that the $\hat{\Phi}_{inf}(\vec{\chi}',0|\vec{\chi},s)$ of Eq. (7) can also be expressed in a much simpler form in spherical coordinates, which is the commonly presented solution of equations like Eq. (6), as

$$\hat{\Phi}_{inf}(\vec{\chi}',0|\vec{\chi},s)=\frac{1}{4\pi D}\frac{1}{|\vec{\chi}-\vec{\chi}'|}\exp\left(-\sqrt{s+\mu_a c}\frac{1}{\sqrt{Dc}}|\vec{\chi}-\vec{\chi}'|\right) \quad (9)$$

The inverse LT of Eq. (9) can be found by using a LT pair [101] of $t^{-3/2}\exp(-a/4t)\overset{LT}{\Leftrightarrow}2\sqrt{\pi}(1/\sqrt{a})\exp(-\sqrt{as})$, the frequency-shifting property of LT, and the time-delay or phase-shifting properties of LT. Thus the time-resolved photon fluence rate in a homogeneous boundless medium, which is the inverse LT of $\hat{\Phi}_{inf}(\vec{\chi}',0|\vec{\chi},s)$ is obtained as [101]

$$\hat{\Phi}_{inf}(\vec{\chi}',0|\vec{\chi},t)=\frac{c}{(4\pi)^{3/2}}\frac{1}{[Dct]^{3/2}}\cdot\exp[-\mu_a ct]\cdot\exp\left(-\frac{1}{4Dct}|\vec{\chi}-\vec{\chi}'|^2\right) \quad (10)$$

An organism under exogenous stress that emits delayed UPE photons for acquisition at the surface of the organism is illustrated schematically in **Figure 2(A)**. The organism for the model purpose is

simplified as a spherical volume, referred to as SOMA, of radius R_0 as shown in Figure 2 (B). A photic source q (unit: W) responsible for UPE photon count detected at the tissue surface is set at $(R_{phot}, \theta', \phi')$.

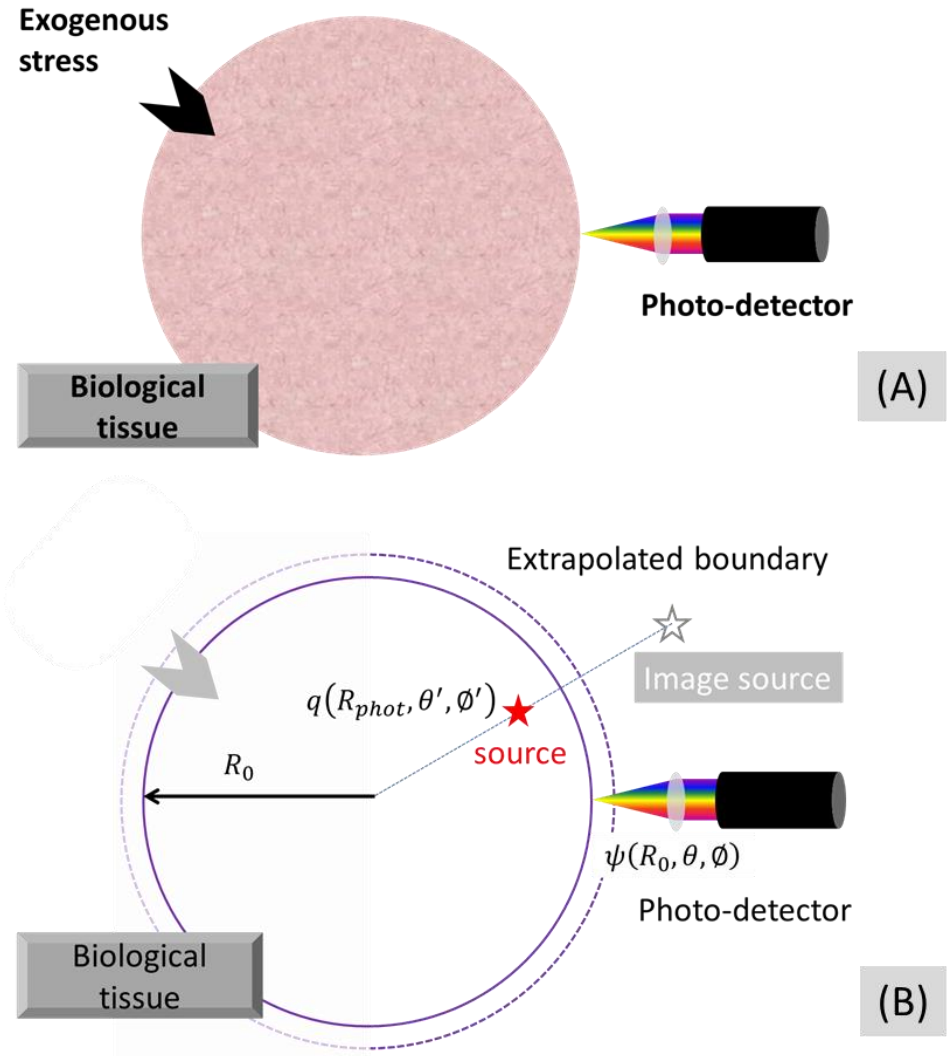

Figure 2. (A) An exogenous stress applied to an organism caused delayed UPE that is measured on the surface of the organism. (B) The acquisition of UPE photons from the organism surface involves a boundary treatment common to diffuse photon measurement.

It must be noted that, the photon emission as a result of complex spatial extension or temporal profile can only be developed when the photon emission in response to a single and simple source is accurately resolved, which is the scope of this work. A site of photo-detection on the tissue surface is set at (R_o, θ, ϕ). With regards to the effect on photon fluence rate by the tissue-air boundary, the photon fluence rate is set zero at a boundary extrapolated at a distance away from the physical boundary of tissue----------the so called extrapolated boundary [102]. For any source within the tissue medium, an "image" of the source is introduced by mirroring the source with respect to the extrapolated boundary that is co-centric with and at a radial distance of $R_b = 2AD$ outward from the physical boundary [100] where $A = (1 + \xi)/(1 - \xi)$, $\xi = -1.440n^{-2} + 0.710n^{-1} + 0.668 + 0.0636n$, and n is the refractive index of the air-bounding tissue. The composite photon fluence rate at the extrapolated boundary that is resulted from both the physical source in the tissue medium and the image of the physical source with respect to the extrapolated boundary is set to zero. Subsequently the composite positive photon fluence rate at the tissue

medium surface is quantifiable by using the same two sources, as governed by the uniqueness property of electromagnetic entities.

For a photo-genic source $\hat{\mathrm{q}}(\vec{\chi}',0)$ located off-center at (R_{phot},θ',ϕ'), the geometric symmetry determines that the image of it with respect to the extrapolated boundary must locate along the same radial direction of it. The source $\hat{\mathrm{q}}(\vec{\chi}',0)$ and its image with respect to the extrapolated boundary collectively set zero the photon fluence rate (as well as its LT) on the extrapolated boundary. Based on Eq. (7), the LT of the photon fluence rate associated with the photo-genic source $\hat{\mathrm{q}}(\vec{\chi}',0)$ and evaluating on the extrapolated boundary, for which the source locates at $r_< = R_{phot}$ and the field point locates at $r_> = R_0 + R_b$, is

$$\hat{\Psi}_{phot}\big|_{ext}(\vec{\chi}',0|\vec{\chi},\mathrm{s}) = \frac{1}{\mathrm{D}}(\hat{\mu}^{\mathrm{s}}_{\mathrm{eff}})\sum_{\mathrm{l}=0}^{\infty}\left\{i_l\left[\hat{\mu}^s_{eff}\cdot(R_{phot})\right]\cdot k_l\left[\hat{\mu}^s_{eff}(R_0+R_b)\right]\right\} \cdot\sum_{\mathrm{m}=-\mathrm{l}}^{\mathrm{l}}[\mathrm{Y}^*_{\mathrm{lm}}(\theta',\phi')\cdot\mathrm{Y}_{\mathrm{lm}}(\theta,\phi)] \quad (11)$$

where the notation "$_{left}\big|_{right}$" indicates evaluating the "left" as the source on the "right" as the field position. Note that any l-th order (or moment) of the photo-genic source $\hat{\mathrm{q}}(\vec{\chi}',0)$ has the same intensity of unity. Similarly, the LT of the photon fluence rate associated with the image of the photo-genic source and evaluating on the extrapolated boundary, for which the source now locates at a radial position of a to-be-determined $r_>$ and the detector locates at $r_< = R_0 + R_b$, is

$$\hat{\Psi}^{imag}_{phot}\big|_{ext}(\vec{\chi}',0|\vec{\chi},\mathrm{s}) = \frac{1}{\mathrm{D}}(\hat{\mu}^{\mathrm{s}}_{\mathrm{eff}})\sum_{\mathrm{l}=0}^{\infty} q^*_l\cdot\left\{i_l\left[\hat{\mu}^s_{eff}\cdot(R_0+R_b)\right]\cdot k_l\left[\hat{\mu}^s_{eff}r_>\right]\right\} \cdot\sum_{\mathrm{m}=-\mathrm{l}}^{\mathrm{l}}[\mathrm{Y}^*_{\mathrm{lm}}(\theta',\phi')\cdot\mathrm{Y}_{\mathrm{lm}}(\theta,\phi)] \quad (12)$$

where the q^*_l terms are dependent upon the order (or moment) l. Based on the essence of "image-source" [35, 36], the two unknown terms q^*_l and $r_>$ associated with the l-th order (or moment) "image" source (the k_l component) can be expressed by a single unknown term q_l associated with the same order (or moment) of the actual photo-genic source $\hat{\mathrm{q}}(\vec{\chi}',0)$ located within the tissue at (R_{phot},θ',ϕ') (the i_l component), as the following:

$$q^*_l\cdot k_l\left[\hat{\mu}^s_{eff}r_>\right] = q_l\cdot i_l\left[\hat{\mu}^s_{eff}(R_{phot})\right] \quad (13)$$

Applying Eq. (12-14) to the condition of extrapolated zero-boundary that sets $\hat{\Psi}_{phot}\big|_{ext}(\vec{\chi}',0|\vec{\chi},\mathrm{s}) + \hat{\Psi}^{imag}_{phot}\big|_{ext}(\vec{\chi}',0|\vec{\chi},\mathrm{s}) = 0$ leads to

$$q_l = -\frac{k_l\left[\hat{\mu}^s_{eff}(R_0+R_b)\right]}{i_l\left[\hat{\mu}^s_{eff}(R_0+R_b)\right]} \quad l = 0,1,2,\ldots \quad (14)$$

Now for the LT of photon fluence rate associated with the photo-genic source at (R_{phot},θ',ϕ'), but evaluating at a field point between the body boundary and the extrapolated boundary, the source still locates at $r_< = R_{phot}$ but the detector or the field point locates at $r_> = R_0 + \Delta r$, where $\Delta r \in [0, R_b]$ (a field point on the body boundary simply corresponds to $r_> = R_0$ or $\Delta r = 0$). For the LT of the photon fluence rate associated with the image of the photo-genetic source and also evaluating at a field point between the body boundary and the extrapolated boundary, the field point now locates at $r_< = R_0 + \Delta r$ and the source terms are known through Eqs. (13) and (14). Collectively the composite LT of the photon fluence rate originating from a photo-genic source at (R_{phot},θ',ϕ') and sensed by a detector or field point at $(R_0 + \Delta r\,,\theta,\phi)$ between the body boundary and the extrapolated boundary becomes:

$$\hat{\Psi}_{\mathrm{SOMA}}(\vec{\chi}',0|\vec{\chi},\mathrm{s}) = \hat{\Psi}_{phot}\big|_{ext}(\vec{\chi}',0|\vec{\chi},\mathrm{s}) + \hat{\Psi}^{imag}_{phot}\big|_{ext}(\vec{\chi}',0|\vec{\chi},\mathrm{s}) =$$

$$= \frac{1}{D}\left(\hat{\mu}^s_{eff}\right)\sum_{l=0}^{\infty} i_l\left[\hat{\mu}^s_{eff}(R_{phot})\right]\cdot k_l\left[\hat{\mu}^s_{eff}(R_0+\Delta r)\right]\sum_{m=-l}^{l} Y^*_{lm}(\theta',\phi')Y_{lm}(\theta,\phi)$$

$$-\frac{1}{D}\left(\hat{\mu}_{eff}^{s}\right)\sum_{l=0}^{\infty}\cdot i_l\left[\hat{\mu}_{eff}^{s}(R_0+\Delta r)\right]i_l\left[\hat{\mu}_{eff}^{s}(R_{phot})\right]\cdot\frac{k_l\left[\hat{\mu}_{eff}^{s}(R_0+R_b)\right]}{i_l\left[\hat{\mu}_{eff}^{s}(R_0+R_b)\right]}\sum_{m=-l}^{l}Y_{lm}^{*}(\theta',\phi')Y_{lm}(\theta,\phi)$$

$$=\frac{1}{D}\left(\hat{\mu}_{eff}^{s}\right)\sum_{l=0}^{\infty}i_l\left[\hat{\mu}_{eff}^{s}(R_{phot})\right]\cdot k_l\left[\hat{\mu}_{eff}^{s}(R_0+\Delta r)\right]\sum_{m=-l}^{l}Y_{lm}^{*}(\theta',\phi')Y_{lm}(\theta,\phi)$$

$$\left\{1-\frac{i_l\left[\hat{\mu}_{eff}^{s}(R_0+\Delta r)\right]}{k_l\left[\hat{\mu}_{eff}^{s}(R_0+\Delta r)\right]}\frac{k_l\left[\hat{\mu}_{eff}^{s}(R_0+R_b)\right]}{i_l\left[\hat{\mu}_{eff}^{s}(R_0+R_b)\right]}\right\} \quad (15)$$

Equation (15) contains two parts: the "1" in the bracket represents the infinite-medium contribution to the LT of the photon fluence rate associated with the photo-genic source $\hat{\mathrm{q}}(\vec{\chi}',0)$ that can be expressed by the alternative simple form of Eq. (6); and the other term in the bracket is the scaling of the infinite-medium contribution to the LT of the photon fluence rate by the image of the photo-genic source $\hat{\mathrm{q}}(\vec{\chi}',0)$ with respect to the former one. By using some analytics of the modified spherical Bessel function and Eq. (14), Eq. (15) is converted to the following form [100]

$$\hat{\Psi}_{SOMA}(\vec{\chi}',0|\vec{\chi},\mathrm{s})=\frac{1}{4\pi D}\frac{1}{\left|\vec{X}-\vec{X}'_{phot}\right|}exp\left(-\hat{\mu}_{eff}^{s}\left|\vec{X}-\vec{X}'_{phot}\right|\right)\left\{1-\frac{I_{l+1/2}\left[\hat{\mu}_{eff}^{s}(R_0+\Delta r)\right]}{K_{l+1/2}\left[\hat{\mu}_{eff}^{s}(R_0+\Delta r)\right]}\frac{K_{l+1/2}\left[\hat{\mu}_{eff}^{s}(R_0+R_b)\right]}{I_{l+1/2}\left[\hat{\mu}_{eff}^{s}(R_0+R_b)\right]}\right\} \quad (16)$$

where $I_{l+\frac{1}{2}}$ and $K_{l+\frac{1}{2}}$ are respectively the $\left(l+\frac{1}{2}\right)$-th order modified Bessel function of the first and the second kinds. This work considers an organism of the size of a human as that will produce much longer delay of photons measured at the surface in comparison to a small organism like a cell, for the purpose of assessing the upper limit of the temporal spread of photons of UPE spectral relevancy that can be caused by tissue scattering. So if the temporal spread of the photon at this large SOMA size is substantially smaller than the temporal scale of the delayed UPE known to the current experimental records, so is the temporal spread of the propagation of UPE photon in any organisms reported. For a human-sized tissue domain, it is easy to have an R_0 (i.e., 10cm) that is substantially greater than 10 times of the magnitude of $1/\hat{\mu}_{eff}^{s}$ to have the second term in the bracket of Eq. (16) approximated by

$$\frac{I_{l+1/2}\left[\hat{\mu}_{eff}^{s}(R_0+\Delta r)\right]}{K_{l+1/2}\left[\hat{\mu}_{eff}^{s}(R_0+\Delta r)\right]}\frac{K_{l+1/2}\left[\hat{\mu}_{eff}^{s}(R_0+R_b)\right]}{I_{l+1/2}\left[\hat{\mu}_{eff}^{s}(R_0+R_b)\right]}=exp\left[-2\hat{\mu}_{eff}^{s}(R_b-\Delta r)\right] \quad (17)$$

which will change Eq. (16) to a trivial form of

$$\hat{\Psi}_{SOMA}(\vec{\chi}',0|\vec{\chi},\mathrm{s})=\frac{1}{4\pi D}\frac{1}{\left|\vec{X}-\vec{X}'_{phot}\right|}exp\left(-\hat{\mu}_{eff}^{s}\left|\vec{X}-\vec{X}'_{phot}\right|\right)\left\{1-exp\left[-2\hat{\mu}_{eff}^{s}(R_b-\Delta r)\right]\right\} \quad (18)$$

Equation (18) that is associated with the photo-genic source $\hat{q}(\vec{\chi}',0)$ conveniently satisfies the condition of producing zero composite LT of the photon fluence rate at the extrapolated boundary whereupon $\Delta r = R_b$. Equation (18) also determines that the LT of the photon fluence rate associated with the photo-genic source $\hat{q}(\vec{\chi}',0)$ decreases monotonically away from the body boundary up to the extrapolated boundary. Similar patterns holds for the photon fluence rate, since LT is a linear transformation. It can be projected that Eq. (18) applies to a source at the center of a spherical tissue domain that is significantly greater than the reduced scattering pathlength.

By using Eq. (8), Eq. (18) evolves to the following:

$$\Psi_{SOMA}(\vec{\chi}',0|\vec{\chi},s)=\frac{1}{4\pi D}\frac{1}{\left|\vec{X}-\vec{X}'_{phot}\right|}\left\{exp\left(-\hat{\mu}_{eff}^{s}\left|\vec{X}-\vec{X}'_{phot}\right|\right)-exp\left\langle-\hat{\mu}_{eff}^{s}\left[\vec{X}-\vec{X}'_{phot}+2(R_b-\Delta r)\right]\right\rangle\right\}$$

$$=\frac{1}{4\pi D}\frac{1}{\left|\vec{X}-\vec{X}'_{phot}\right|}\left\{exp\left(-\sqrt{s+\mu_a c}\frac{1}{\sqrt{Dc}}\left|\vec{X}-\vec{X}'_{phot}\right|\right)-exp\left\langle-\sqrt{s+\mu_a c}\frac{1}{\sqrt{Dc}}\left[\left|\vec{X}-\vec{X}'_{phot}\right|+2(R_b-\Delta r)\right]\right\rangle\right\} \quad (19)$$

And implementation of Eq. (9) with Eq. (19) leads to the time-resolved photon fluence rate measured at the surface of a spherical tissue domain significantly greater than the reduced scattering pathlength of the tissue in response to a spatially and temporally impulse photon source of unity intensity within the tissue as the following:

$$\widehat{\Psi}_{SOMA}(\vec{\chi}', 0|\vec{\chi}, t) = \frac{c}{(4\pi)^{3/2}} \frac{1}{[Dct]^{3/2}} \cdot \exp[-\mu_a ct] \cdot \langle \exp\left(-\frac{1}{4Dct}\left|\vec{X} - \vec{X}'_{phot}\right|^2\right) - \exp\left\{-\frac{1}{4Dct}\left[\left|\vec{X} - \vec{X}'_{phot}\right| + 2(R_b - \Delta r)\right]^2\right\}\rangle \quad (20)$$

Equation (20) is the temporal point-spread function or temporal impulse response of the spherical tissue medium when evaluating time-resolved diffusion of photons originating from the center of the spherical tissue domain.

3.2 Estimation of the temporal spread of light of UPE spectral relevancy in a spherical tissue volume of up to 40cm in diameter due to photon diffusion

Equation (20) is implemented to assess the temporal spread of a light impulse of UPE spectral relevancy, after experiencing diffusion in a highly scattering tissue domain of 20cm or 40cm in diameter. The 40cm diameter is comparable to the cross-sectional size of an adult human. The refractive index of the tissue is set as 1.40. Because tissue absorption does not contribute to the temporal spread, an absorption coefficient of $\mu_a = 0.1cm^{-1}$ that is representative of a bulk biological tissue at the VIS-NIR band [103] is assigned to the homogeneous tissue domain. The reduced scattering coefficient of the tissue is set at three values: $10cm^{-1}$, $100cm^{-1}$, and $500cm^{-1}$. Among these three values of the reduced scattering coefficient, $10cm^{-1}$ can be easily found with a biological tissue [103], but $500cm^{-1}$ may be too strong to be associated with any biological tissues [104]. The temporal spread caused by an extremely strong reduced scattering coefficient of $500cm^{-1}$ will thus set the limit of the temporal spread that cannot be surpassed by the photon diffusion process, when UPE photons have to traverse from a site of photo-genesis within the tissue to a surface site of measurement.

The temporal spread function of Eq. (20) evaluated for the spherical tissue domains of 2 sizes and 3 values of reduced scattering coefficient are displayed in **Figure 3**, after normalizing to the peak value of each. The (A) and (B) correspond to a tissue size of a radius of 10cm or a diameter of 20cm. The (C) and (D) refer to the tissue size of a radius of 20cm or a diameter of 40cm. The time-resolved photon fluence rate being the ordinate is displayed at a linear scale in (A) or (C), and a logarithmic scale in (B) or (D). The range of the ordinates representing the photon fluence rate (equivalently the photon count) in (B) and (D) are limited to 10 orders of magnitude, which however well exceeds the experimental dynamic ranges (6 orders of magnitude) of detecting delayed UPE [34]. Figure 3 demonstrates that, as photons of UPE spectral relevancy diffuse in tissue over a line-of-sight distance of 20cm that is comparable to the distance from the cross-sectional center of a human-size tissue to the cross-sectional edge, an extremely high values of tissue reduced scattering coefficient of $500cm^{-1}$ that is about 50 times stronger than the reduced scattering coefficient of typical soft biological tissues will produce a temporal spread of less than 90ns. The 90ns spread equates to a total photon path-length of less than 20 meters in tissue. It is noted that this 90ns maximal temporal spread is also associated with a dynamic range of 10 orders of magnitude that is at least 4 orders of magnitude greater than the instrument responses used for detecting delayed UPE in 60 strong reports surveyed in Table 1. Therefore it can be projected that, any photon emission of delayed UPE from organisms that has a delay time longer than 100ns after the removal of the stress cannot be accounted for by the temporal broadening of the photon pack due to tissue scattering.

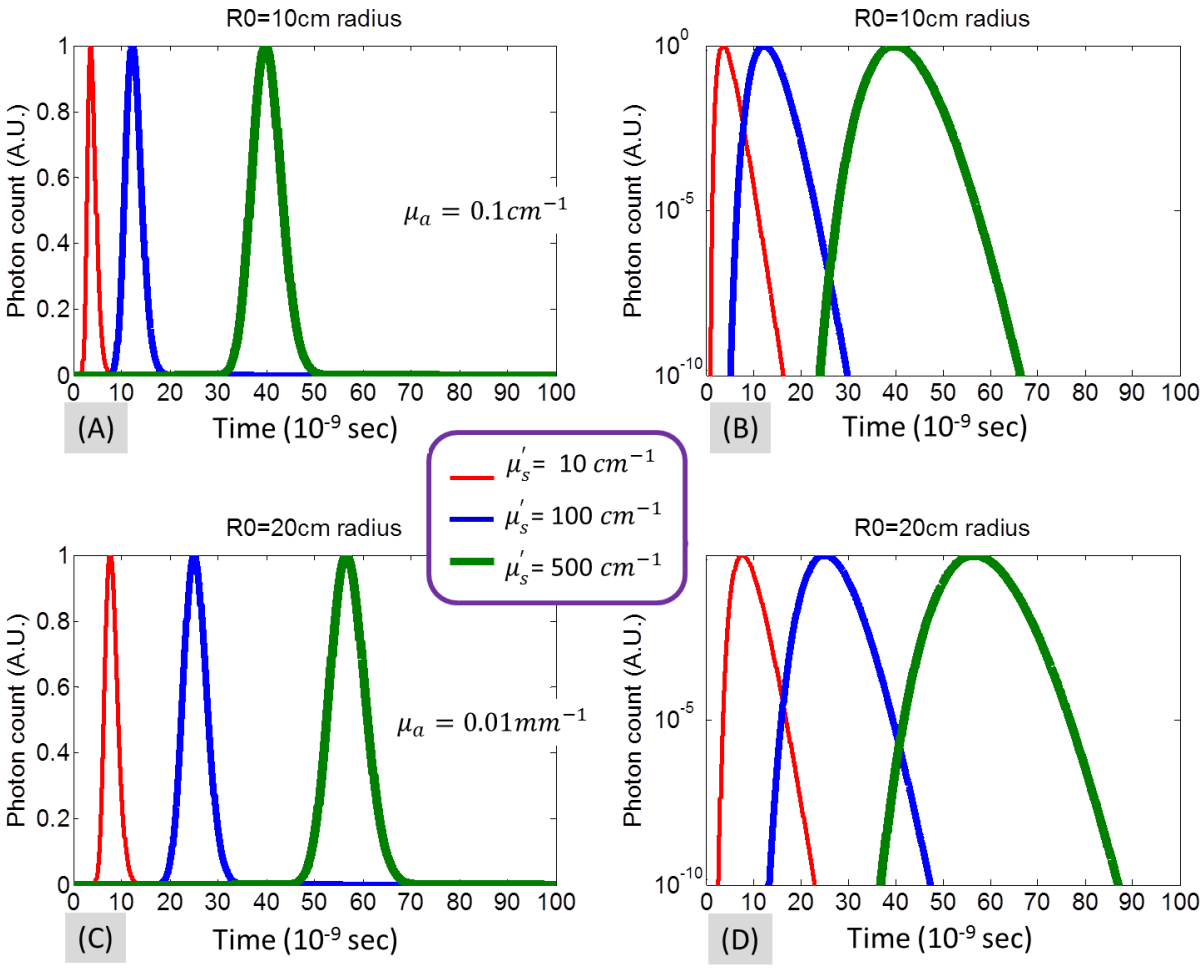

Figure 3. The temporal spread of the photon fluence rate measured at the surface of a spherical tissue domain of 40cm in dimeter, in response to a spatially and temporally impulsive source at the center of the spherical tissue domain.

4. The stress-transfer pathway hypothesized to source the photons detected as delayed UPE at a rate much slower than the lifetime of photon propagation before surface emission

The survey in the previous section 2 has identified the shortest delay time of delayed UPE to be 8.5μs. This shortest temporal delay of delayed UPE is nearly two orders of magnitude longer than the upper limit of the temporal spreading of photon propagation in tissue that could be caused by tissue scattering. The delay time of delayed UPE is the temporal spread of the photons measured on the tissue surface with respect to the instant of stress removal. A temporal spread of photons that is much later and longer than that can be caused by scattering associated photon diffusion can only be explained by a slower and longer (if not retarded) process of the photons being produced, since each photon of delayed UPE detected at the tissue surface comes from a source and the photons must have traversed through the tissue to the surface room that source. This slower sourcing of the photons in responding to a stress that have traversed through the tissue to the surface for being detected as delayed UPE is schematically illustrated in **Figure 4**. The photons emitted by any source in tissue and reaching the site of detection at the surface may diffuse in tissue over a distance much longer than a ballistic line-of-sight path between the source position and the detector position due to tissue scattering, but the scattering-caused temporal delay happens at light speed. This light-speed photon-diffusion when associated with a slower or longer production of the photons at the source position will cause the temporal profile of the surface detected photons to change at a later time and over a longer duration.

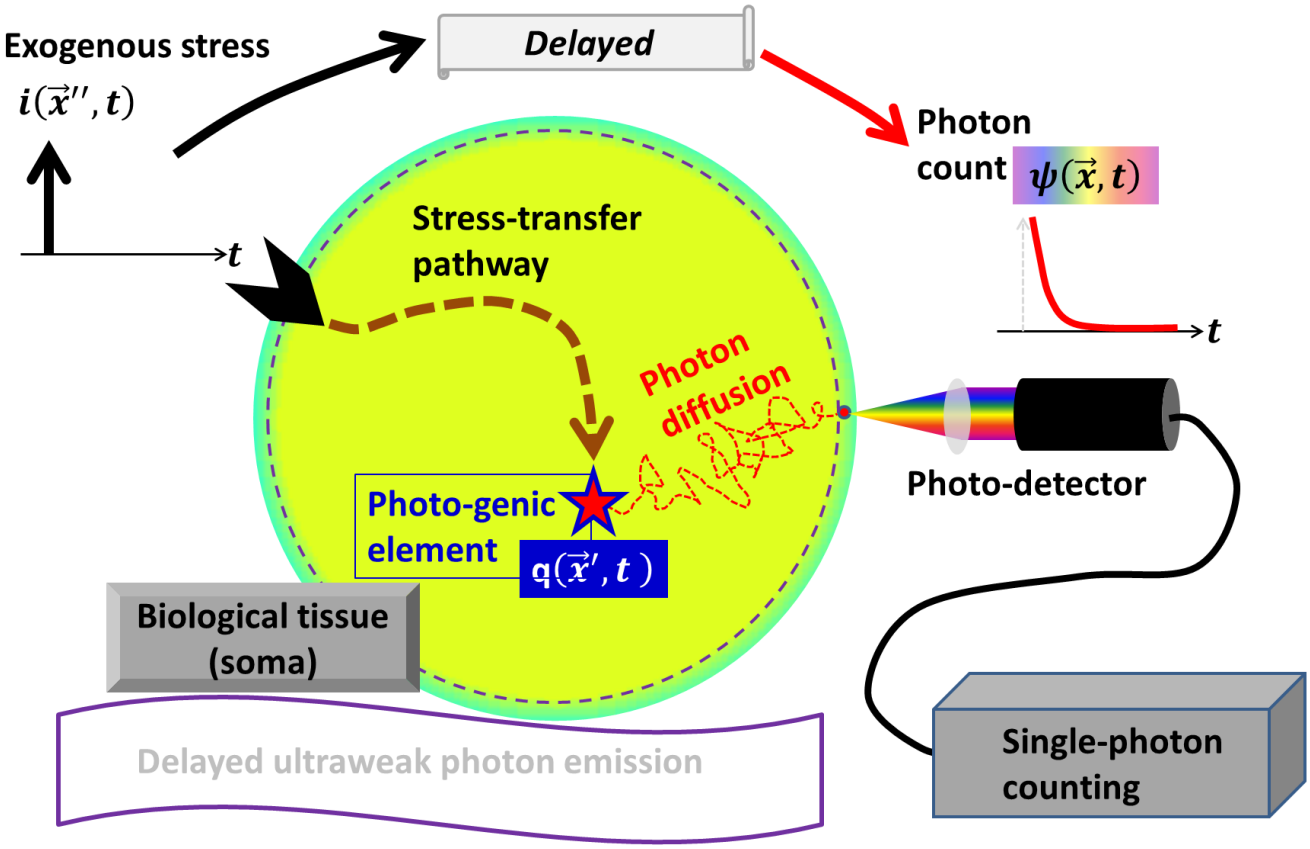

Figure 4. A slower process of photo-genesis in response to stress is hypothesized to precede the photon diffusion in tissue. This is because even the minimal delay of 8.5μs of the delayed UPE cannot be attributed to the temporal broadening that must occur to the UPE photons due to tissue scattering.

In the case of slow photon sourcing, the temporal profile of the photons measured at the tissue surface is the convolution of the source temporal profile with the temporal point-spread function $\hat{\Psi}_{SOMA}(\vec{\chi}', 0|\vec{\chi}, t)$ of the photon diffusion process. When the temporally spread source at $\vec{\chi}'$ is spatially impulsive as $\hat{q}(\vec{\chi}', t) = q(t)$, $t \geq 0$, the convolution results in the following:

$$\boxed{\hat{\Psi}_{Delay}(\vec{\chi}', t|\vec{\chi}, t)} = \hat{\Psi}_{SOMA}(\vec{\chi}', 0|\vec{\chi}, t) \circledast \hat{q}(\vec{\chi}', t) = \int_{-\infty}^{t} \hat{\Psi}_{SOMA}(\vec{\chi}', 0|\vec{\chi}, \tau) \cdot q(t-\tau) d\tau \quad (21)$$

When the temporally spread source at $\vec{\chi}'$ is also spatially spread, $\hat{q}(\vec{\chi}', t) = Q(\vec{\chi}')q(t)$, $t \geq 0$, the spatial convolution will also be involved in finding the temporal profile of the photons detected at the tissue surface as the following:

$$\begin{aligned} \boxed{\hat{\Psi}_{Delay}(\vec{\chi}', t|\vec{\chi}, t)} &= \hat{\Psi}_{SOMA}(\vec{\chi}', 0|\vec{\chi}, t) \circledast \hat{q}(\vec{\chi}', t) \\ &= \int_{-\infty}^{+\infty} Q(\vec{\chi}' - x) \cdot \left[\int_{-\infty}^{t} \hat{\Psi}_{SOMA}(x, 0|\vec{\chi}, \tau) \cdot q(t-\tau) d\tau \right] dx \end{aligned} \quad (22)$$

Equation (22) will be relevant if the spatial extent of the entity that sources the delayed UPE is known-----a topic that is prohibiting at the present because of the lack of mechanistic discoveries. This work limits the discussion of photo-genesis to be spatially impulsive to use Eq. (21) to determine the temporal profile of the photons detected at the tissue surface as delayed UPE. For a temporal impulse response $\hat{\Psi}_{SOMA}(\vec{\chi}', 0|\vec{\chi}, t)$ that is significantly faster (i.e., 100 times faster) than the temporal profile of the source generation $\hat{q}(\vec{\chi}', t) = q(t)$, the temporal impulse response $\hat{\Psi}_{SOMA}(\vec{\chi}', 0|\vec{\chi}, t)$ can be approximated as a Dirac delta function for the convolution. And the temporal profile of the outcome of the convolution of any function with a Dirac delta function will be dictated by the temporal profile of the function. In

referring to the previous section and Figure 3, one can find that the temporal spread expected for photons propagating over a line-of-sight distance of 20cm in a tissue of extremely high reduced scattering coefficient of $500cm^{-1}$ with a detection dynamic range of 6-orderes of magnitude is less than 80ns. The shortest delay time of 8.5μs of delayed UPE is >100 times longer than the 80ns temporal spread that is practically the upper limit of the temporal scale of $\widehat{\Psi}_{SOMA}(\vec{\chi}', 0|\vec{\chi}, t)$. Therefore the temporal profile of delayed photon acquisition at delay times longer than 8.5μs will faithfully follow the temporal profile of the photon generation of $\hat{q}(\vec{\chi}', t) = \mathbb{q}(t)$. For this reason, the subsequent analysis is restricted to the kinetics of photo-genesis of $\hat{q}(\vec{\chi}', t) = \mathbb{q}(t)$.

The photon-genesis process that sources the photons emitted as delayed UPE would be associated with the metabolic pathway that responds to an external stress that perturbs the homeostatic tissue or organism. The metabolic response to the external stress up to the photo-genesis is considered to form a stress-transfer pathway that determines the rate of producing the photons that propagate in tissue before emitting from the tissue surface for being detected. The mechanistic pathways of transforming a stress to photo-genesis are far from being understood [1, 2], therefore it is impractical at the current stage to specify and model any pathways involved more realistically than a linear time-invariant system. Because the response to the stress perturbation to homeostasis is likely presented ultimately at the systematic level, photo-genesis may also occur in a large if not infinite number of tissue sites at any given instant. For modeling purpose, it will only be practical to start with a simple configuration of the photo-genesis that occurs at one site, as illustrated in Fig. 4. The site of photo-genesis is to receive the stress exerted at a different spatial site, through a stress-transfer pathway that converts the stress to photo-genesis at a rate much slower than the life-time of photo propagation in tissue.

The temporal profiles of any stress exerted on an organism can be represented by the individual or linear combination of the profiles presented in **Figure 5**. The (A) represents a single bolus stimulation of a stress intensity of A_{stress} expressed as:

$$i_{bolus}(\vec{\chi}'', t') = A_{stress} \cdot \delta(\vec{\chi} - \vec{\chi}'') \cdot \delta(t') \tag{23}$$

The (B) represents a bolus stimulation of a stress intensity of A_{stress} that is applied repetitively at an interval of T for a total of N times as expressed by:

$$i_{bolus}^{rep}(\vec{\chi}'', t') = A_{stress} \cdot \delta(\vec{\chi} - \vec{\chi}'') \cdot \sum_{n=0}^{N} \delta(t' - nT) = \sum_{n=0}^{N} i_{bolus}[\vec{\chi}'', (t' - nT)] \tag{24}$$

The (C) denotes a continuous stimulation of a stress intensity of A_{stress} characterized by

$$i_{step}(\vec{\chi}'', t') = A_{stress} \cdot \delta(\vec{\chi} - \vec{\chi}'') \cdot u(t') \tag{25}$$

where $u(t')$ is the Heaviside function. The (D) represents a stimulation of a stress intensity of A_{stress} that is applied over a duration of ΔT as is expressed by:

$$i_{pulse}(\vec{\chi}'', t') = A_{stress} \cdot \delta(\vec{\chi} - \vec{\chi}'') \cdot [u(t') - u(t' - \Delta T)] = i_{step}(\vec{\chi}'', t') - i_{step}[\vec{\chi}'', (t' - \Delta T)] \tag{26}$$

The (E) represents a stimulation of a stress intensity of A_{stress} that is applied over a duration of ΔT and repeated with an interval of T for a total of N times, which is expressed by:

$$i_{pulse}^{rep}(\vec{\chi}'', t') = A_{stress} \cdot \delta(\vec{\chi} - \vec{\chi}'') \cdot \sum_{n=0}^{N}[u(t' - nT) - u(t' - \Delta T - nT)]$$
$$= \sum_{n=0}^{N} i_{pulse}[\vec{\chi}'', (t' - nT)] \quad = \sum_{n=0}^{N}\{i_{step}[\vec{\chi}'', (t' - nT)] - i_{step}[\vec{\chi}'', (t' - \Delta T - nT)]\} \tag{27}$$

The impulse response of the stress-transfer pathway that transfers the stress occurring at a spatial location of $\vec{\chi}''$ to the photo-genesis at a different location of $\vec{\chi}'$ is denoted as $\hbar_{stress}(\vec{\chi}'' \Rightarrow \vec{\chi}', t')$. The response of the stress-transfer pathway to any input of $i_{stress}(\vec{\chi}'', t')$ is the convolution of the stress with the impulse response and that becomes the intensity profile of the photon source as

$$q(\vec{\chi}', t') = i_{stress}(\vec{\chi}'', t') \circledast \hbar_{stress}(\vec{\chi}'' \Rightarrow \vec{\chi}', t') = \int_0^{t'} i_{stress}(\vec{\chi}'', \beta) \cdot \hbar_{stress}[\vec{\chi}'' \Rightarrow \vec{\chi}', (t' - \beta)]d\beta \tag{28}$$

The photo-genesis in response to a bolus input represented by Eq. (23) is thus

$$q_{bolus}(\vec{\chi}', t') = i_{boluss}(\vec{\chi}'', t') \circledast \hbar_{stress}(\vec{\chi}'' \Rightarrow \vec{\chi}', t') \tag{29}$$

The photo-genesis in response to a repetitive bolus input represented by Eq. (24) is then

$$q_{bolus}^{rep}(\vec{\chi}'', t') = \sum_{n=0}^{N} q_{bolus}[\vec{\chi}'', (t' - nT)] \quad (30)$$

The photo-genesis in response to a step input represented by Eq. (25) is the following

$$q_{step}(\vec{\chi}', t') = i_{step}(\vec{\chi}'', t') \circledast \hbar_{stress}(\vec{\chi}'' \Rightarrow \vec{\chi}', t') \quad (31)$$

The photo-genesis in response to a pulse input represented by Eq. (26) becomes

$$q_{pulse}(\vec{\chi}'', t') = q_{step}(\vec{\chi}'', t') - q_{step}[\vec{\chi}'', (t' - \Delta T)] \quad (32)$$

The photo-genesis in response to a repetitive pulse input represented by Eq. (27) evolves as

$$\begin{aligned} q_{pulse}^{rep}(\vec{\chi}'', t') &= \sum_{n=0}^{N} q_{pulse}[\vec{\chi}'', (t' - nT)] \\ &= \sum_{n=0}^{N} \{q_{step}[\vec{\chi}'', (t' - nT)] - q_{step}[\vec{\chi}'', (t' - \Delta T - nT)]\} \end{aligned} \quad (33)$$

It is straightforward to conclude from Eqs (29)-(33) that the system's outputs to a bolus stress as well as a step stress characterize the responses of the system to more complex inputs that can be decomposed to a linear combination of bolus and step patterns. Therefore the following section restricts the analysis to the stress-transfer pathway pertinent to a bolus input of Eq. (23) using the convolution principle of Eq. (29) and a step input of Eq. (25) using the convolution principle of Eq. (31).

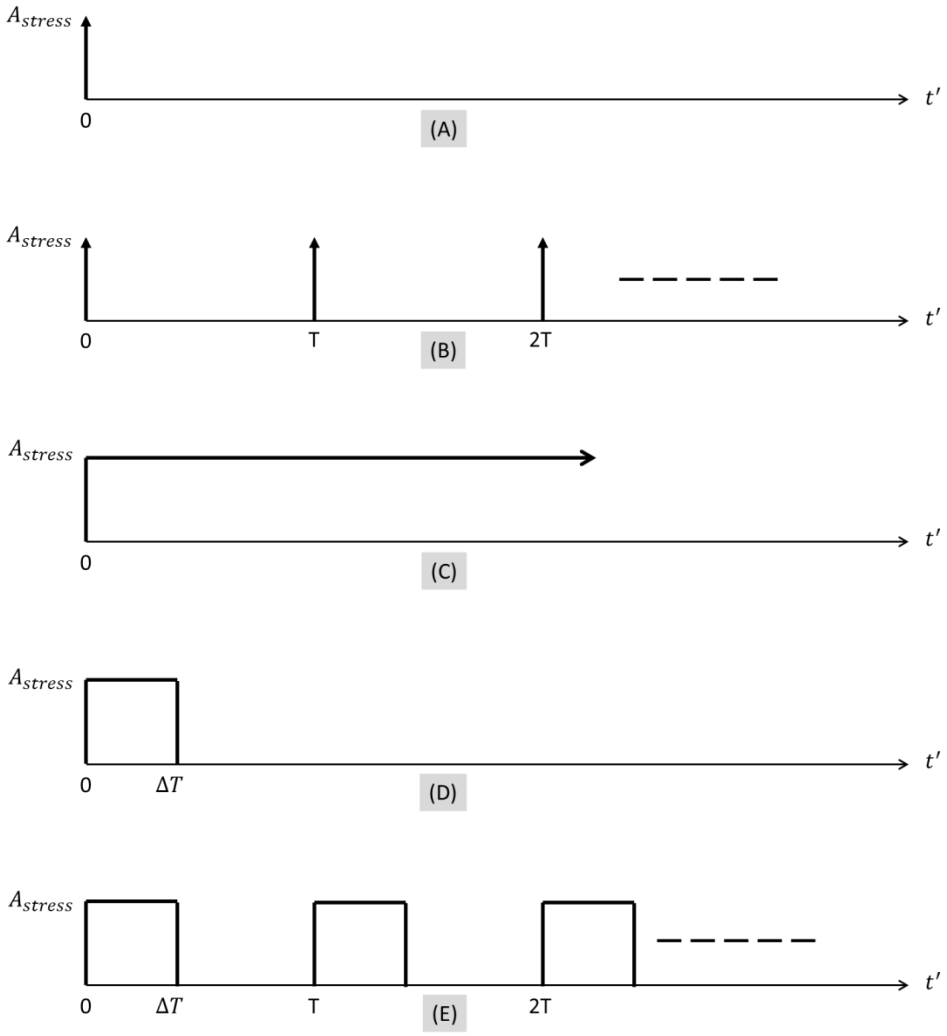

Figure 5. The temporal profile of a few simple stress pattern: (A) bolus; (B) repeated bolus; (C) step, (D) pulse, (E) repeated pulse.

4.1 Stress-transfer pathway hypothesized to present a single first-order low-pass response:

Compartmental analyses of kinetics of various body functions have indicated low-pass pattern to be common for physiological or metabolic responses to external perturbations [105]. A first-order low-pass

response is thus modeled as the simplest pathway linking the external stress and the source of UPE photons or the site of photo-genesis as shown in **Figure 6**. The external stress is assumed to be applied at a spatial location of $\vec{\chi}''$ and an instant of t' as represented by $i_{stress}(\vec{\chi}'', t')$. This stress is considered to cause a change to a potential of metabolic aspect (or a metabolic potential) at a spatial location of $\vec{\chi}'$ and the same instant of t' that is represented by $\circledcirc_1(\vec{\chi}', t')$, at a kinetic rate of $K_{01}(\vec{\chi}'' \Rightarrow \vec{\chi}')$ (1/second). The change of the metabolic potential $\circledcirc_1(\vec{\chi}', t')$ is considered photo-genetic, that is to produce photons at the spatial location of $\vec{\chi}'$ with a kinetic rate of $K_{1\mho}(\vec{\chi}')$ (1/second) from which the photons traverse to the surface to be detected as delayed UPE.

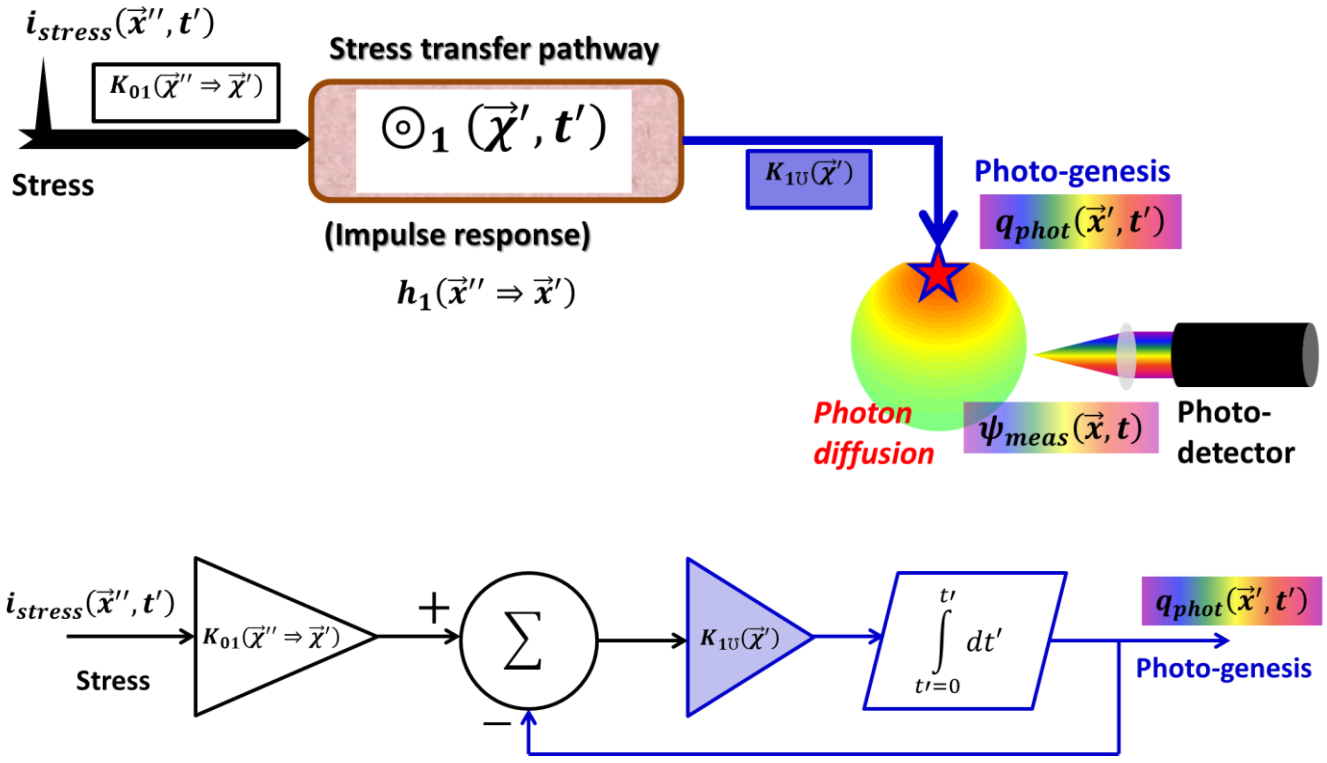

Figure 6. A stress-transfer pathway modeled to present a single first-order low-pass response characterized by constant kinetic rate. The upper level is a schematic and the lower panel corresponds to a system-block diagram.

The transfer structure illustrated in the upper panel of Figure 6 results in the following coupled equations of the kinetic changes:

$$\frac{d}{dt'}\circledcirc_1(\vec{\chi}', t') = K_{01}(\vec{\chi}'' \Rightarrow \vec{\chi}') \cdot i_{stress}(\vec{\chi}'', t') - K_{1\mho}(\vec{\chi}') \cdot \circledcirc_1(\vec{\chi}', t') \tag{34}$$

$$\mathrm{q}_{phot}(\vec{\chi}', t') = K_{1\mho}(\vec{\chi}') \cdot \circledcirc_1(\vec{\chi}', t') \tag{35}$$

If denoting the Laplace transform (LT) of $\mathrm{q}_{phot}(\vec{\chi}', t')$ as $\mathrm{Q}_{phot}(\vec{\chi}', s)$, and the LT of $i_{stress}(\vec{\chi}'', t')$ as $I_{stress}(\vec{\chi}'', s)$, Eqs. (34) and (35) result in a transfer function of the pathway as the following

$$\mathcal{H}_{stress}(\vec{\chi}'' \Rightarrow \vec{\chi}', s) = \frac{\mathrm{Q}_{phot}(\vec{\chi}', s)}{I_{stress}(\vec{\chi}'', s)} = K_{01}(\vec{\chi}'' \Rightarrow \vec{\chi}') \cdot \frac{K_{1\mho}(\vec{\chi}')}{s + K_{1\mho}(\vec{\chi}')} \tag{36}$$

which is a low-pass filter with a pass-band gain of $K_{01}(\vec{\chi}'' \Rightarrow \vec{\chi}')$ and a cut-off frequency at $K_{1\mho}(\vec{\chi}')$. This transfer pathway can also be represented by the system block-diagram of the low panel of Fig. 6. The inverse LT of the transfer function represented by Eq. (36), or the impulse response of the system is:

$$\hbar_{stress}(\vec{\chi}'' \Rightarrow \vec{\chi}', t') = K_{01}(\vec{\chi}'' \Rightarrow \vec{\chi}') \cdot K_{1\mho}(\vec{\chi}') \cdot e^{-K_{1\mho}(\vec{\chi}') \cdot t'} \cdot u(t') \tag{37}$$

The response of this pathway to a bolus stress of magnitude A_{stress} represented by Eq. (23) is simply

$$q^1_{bolus}(\vec{\chi}',t') = [A_{stress}\cdot\delta(\vec{\chi}-\vec{\chi}'')\cdot K_{01}(\vec{\chi}''\Rightarrow\vec{\chi}')\cdot K_{1\upsilon}(\vec{\chi}')]\cdot e^{-K_{1\upsilon}(\vec{\chi}')\cdot t'}\cdot u(t') \quad (38)$$

And the response of this pathway to a step stress of magnitude A_{stress} represented by Eq. (25) is

$$q^1_{step}(\vec{\chi}',t') = [A_{stress}\cdot\delta(\vec{\chi}-\vec{\chi}'')\cdot K_{01}(\vec{\chi}''\Rightarrow\vec{\chi}')]\cdot\left[1-e^{-K_{1\upsilon}(\vec{\chi}')\cdot t'}\right]u(t') \quad (39)$$

4.2 Stress-transfer pathway characterized by dual in-parallel first-order low-pass responses:

A stress-transfer pathway consisting of two in-parallel systems, each presenting a first-order low-pass response is illustrated in **Figure 7**. The transfer function of this system configuration is simply:

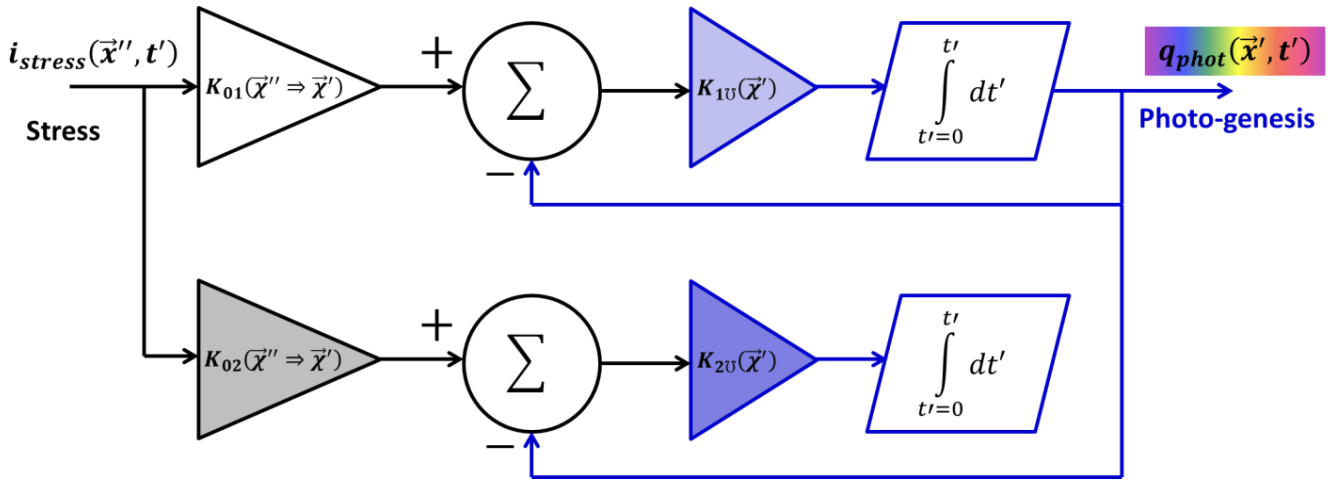

Figure 7. A stress-transfer pathway modeled to present a response that is the combination of two in-parallel first-order low-pass responses characterized by constant kinetic rates.

$$\mathcal{H}_{stress}(\vec{\chi}''\Rightarrow\vec{\chi}',s) = \frac{Q_{phot}(\vec{\chi}',s)}{I_{stress}(\vec{\chi}'',s)} = \sum_{m=1}^{2} K_{0m}(\vec{\chi}''\Rightarrow\vec{\chi}')\cdot\frac{K_{m\upsilon}(\vec{\chi}')}{s+K_{m\upsilon}(\vec{\chi}')} \quad (40)$$

which corresponds to an impulse response of:

$$\hbar_{stress}(\vec{\chi}''\Rightarrow\vec{\chi}',t') = \sum_{m=1}^{2}\left[K_{0m}(\vec{\chi}''\Rightarrow\vec{\chi}')\cdot K_{m\upsilon}(\vec{\chi}')\cdot e^{-K_{m\upsilon}(\vec{\chi}')\cdot t'}\right]\cdot u(t') \quad (41)$$

The response of this pathway to a bolus stress of magnitude A_{stress} represented by Eq. (23) is

$$q^2_{bolus}(\vec{\chi}',t') = A_{stress}\cdot\delta(\vec{\chi}-\vec{\chi}'')\cdot\sum_{m=1}^{2}\left[K_{0m}(\vec{\chi}''\Rightarrow\vec{\chi}')\cdot K_{m\upsilon}(\vec{\chi}')\cdot e^{-K_{m\upsilon}(\vec{\chi}')\cdot t'}\right]\cdot u(t') \quad (42)$$

And the response of this pathway to a step stress of magnitude A_{stress} represented by Eq. (25) is

$$q^2_{step}(\vec{\chi}',t') = A_{stress}\cdot\delta(\vec{\chi}-\vec{\chi}'')\cdot\sum_{m=1}^{2}\left\{K_{0m}(\vec{\chi}''\Rightarrow\vec{\chi}')\cdot\left[1-e^{-K_{m\upsilon}(\vec{\chi}')\cdot t'}\right]\right\}u(t') \quad (43)$$

4.3 Stress-transfer characterized by multiple in-parallel first-order low-pass responses:

Delayed UPE in response to photic-stimulation is well-known to decay hyperbolically. The hyperbolic pattern from mitochondria respiratory complex I in response to photic-stimulation is however shown to be fitted by 4 or 7 exponential functions. According to the discussions to be presented later, a hyperbolic function that decays faster than a exponential function can be decomposed to exponential functions. Therefore, this work uses multiple in-parallel first-order low-pass responses to demonstrate hyperbolic-like responses of the stress-transfer system. A stress-transfer pathway consisting of three or more in-parallel systems, each presenting a first-order low-pass response is illustrated in **Figure 8**. This configuration produces a transfer function of:

$$\mathcal{H}_{stress}(\vec{\chi}''\Rightarrow\vec{\chi}',s) = \frac{Q_{phot}(\vec{\chi}',s)}{I_{stress}(\vec{\chi}'',s)} = \sum_{m=1}^{M} K_{0m}(\vec{\chi}''\Rightarrow\vec{\chi}')\cdot\frac{K_{m\upsilon}(\vec{\chi}')}{s+K_{m\upsilon}(\vec{\chi}')} \quad (44)$$

that corresponds to an impulse response of:

$$\hbar_{stress}(\vec{\chi}''\Rightarrow\vec{\chi}',t') = \sum_{m=1}^{M}\left[K_{0m}(\vec{\chi}''\Rightarrow\vec{\chi}')\cdot K_{m\upsilon}(\vec{\chi}')\cdot e^{-K_{m\upsilon}(\vec{\chi}')\cdot t'}\right]\cdot u(t') \quad (45)$$

The response of this pathway to a bolus stress of magnitude A_{stress} represented by Eq. (23) is

$$q_{bolus}^{M}(\vec{\chi}', t') = A_{stress} \cdot \delta(\vec{\chi} - \vec{\chi}'') \cdot \sum_{m=1}^{M} \left[K_{0m}(\vec{\chi}'' \Rightarrow \vec{\chi}') \cdot K_{m\upsilon}(\vec{\chi}') \cdot e^{-K_{m\upsilon}(\vec{\chi}') \cdot t'} \right] \cdot u(t') \quad (46)$$

The response of this pathway to a step stress of magnitude A_{stress} represented by Eq. (25) is

$$q_{step}^{M}(\vec{\chi}', t') = A_{stress} \cdot \delta(\vec{\chi} - \vec{\chi}'') \cdot \sum_{m=1}^{M} \left\{ K_{0m}(\vec{\chi}'' \Rightarrow \vec{\chi}') \cdot \left[1 - e^{-K_{m\upsilon}(\vec{\chi}') \cdot t'} \right] \right\} u(t') \quad (47)$$

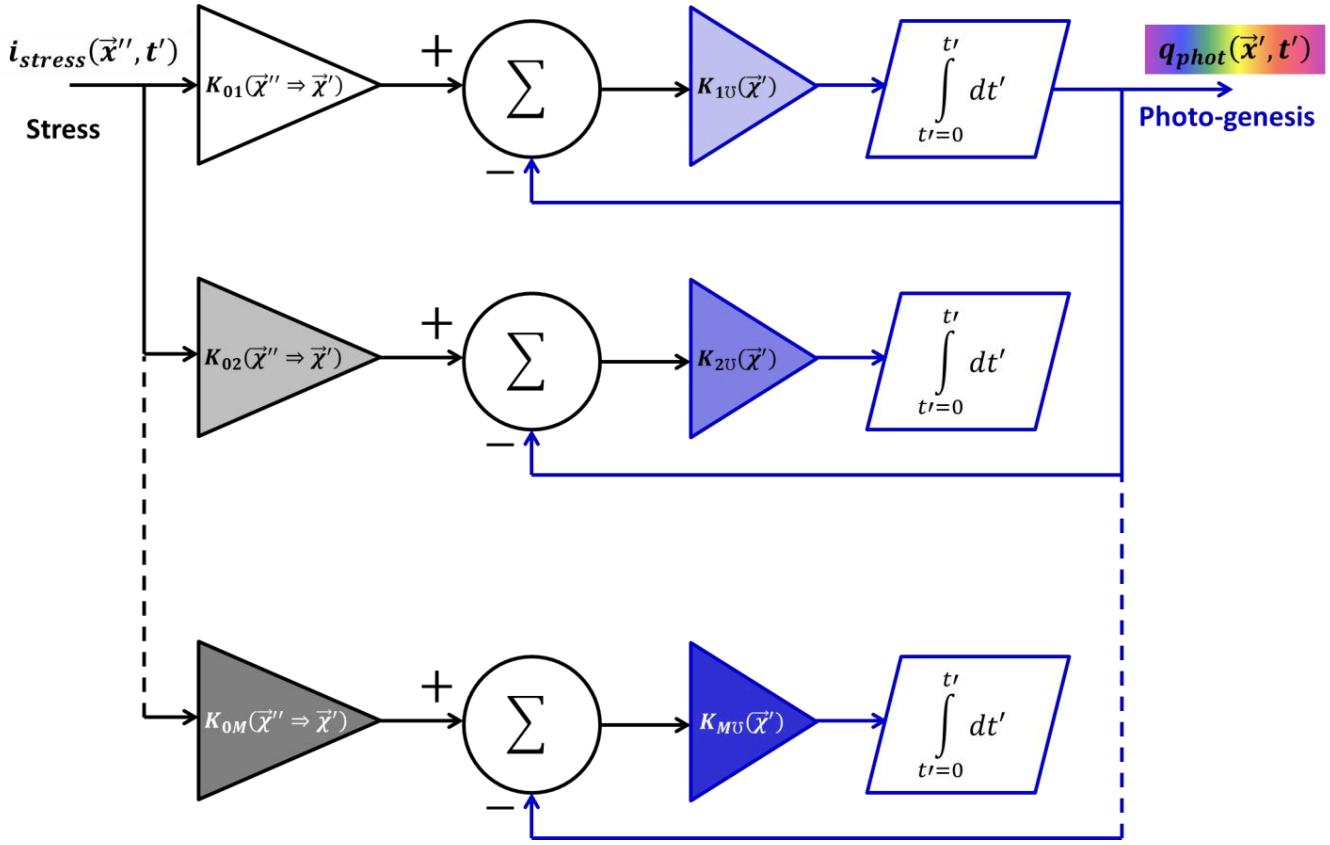

Figure 8. A stress-transfer pathway modeled to present a response that is the combination of three or more in-parallel first-order low-pass responses characterized by constant kinetic rates.

4.4. Stress transfer characterized by first-order low-pass response having slowly varying kinetic rate

A first-order system with a time-varying kinetic rate has been shown applicable to modeling a number of biological rate changes including fluorescence decay lasting less than 35ns [106]. Similar kinetics governed by slowly time-varying rates has been found for delayed fluorescence resulting from triplet-triplet annihilation in polyphenyl quinnoxalines in frozen solutions or films, and phosphorescence intensity decay of strontinum sulfide with the delay recorded over 2000 seconds [107]. The varying kinetic rate fitting the biological responses well has been associated with a lifetime distribution following a gamma function. It has been suggested that this type of slowly varying kinetics within a first-order response may be applicable to a great variety of other biological systems, including delayed UPE. A stress-transfer pathway that has a slowly varying kinetic rate governing the first-order low-pass response is shown in **Figure 9**. It is similar to the single low-pass system shown in Fig. 6 except that it contains a slowly varying kinetic rate operator between the summer and the first-order derivative of the output. The impulse response of this system can be derived as

$$\hbar_{stress}(\vec{\chi}'' \Rightarrow \vec{\chi}', t') = K_{01}(\vec{\chi}'' \Rightarrow \vec{\chi}') \cdot K_{1\upsilon}(\vec{\chi}', t') \cdot e^{-K_{1\upsilon}(\vec{\chi}', t') \cdot t'} \cdot u(t') \quad (48)$$

The response of this pathway to a bolus stress of magnitude A_{stress} represented by Eq. (23) is

$$q_{bolus}^{\tau(t')}(\vec{\chi}', t') = [A_{stress} \cdot \delta(\vec{\chi} - \vec{\chi}'') \cdot K_{01}(\vec{\chi}'' \Rightarrow \vec{\chi}') \cdot K_{1\upsilon}(\vec{\chi}', t')] \cdot e^{-K_{1\upsilon}(\vec{\chi}', t') \cdot t'} \cdot u(t') \quad (49)$$

The response of this pathway to a step stress of magnitude A_{stress} represented by Eq. (25) can be developed by convolving $\hbar_{stress}(\vec{\chi}'' \Rightarrow \vec{\chi}', t')$ of Eq. (48) with $i_{step}(\vec{\chi}'', t')$ of Eq. (25) and that leads to

$$q_{step}^{\tau(t')}(\vec{\chi}', t') = [A_{stress} \cdot \delta(\vec{\chi} - \vec{\chi}'') \cdot K_{01}(\vec{\chi}'' \Rightarrow \vec{\chi}')] \cdot \left[1 - e^{-K_{1\upsilon}(\vec{\chi}', t') \cdot t'}\right] u(t') \quad (50)$$

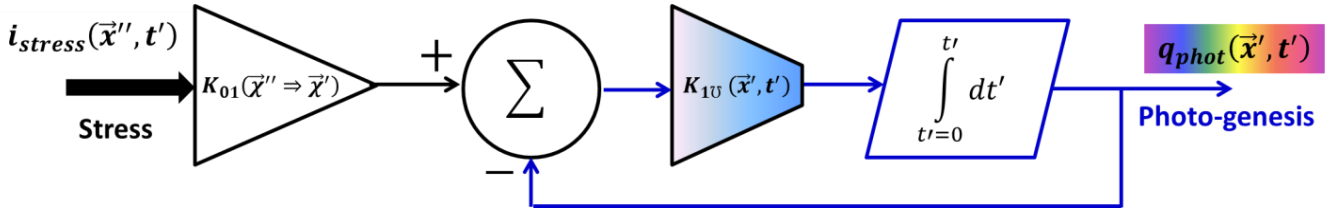

Figure 9. A stress-transfer pathway modeled to present a single first-order low-pass response characterized by varying kinetic rate.

4.6. Stress transfer characterized by a second-order low-pass response

A stress-transfer pathway hypothesized to present a second-order low-pass response is illustrated in **Figure 10**. The system contains two kinetic rates in terms of the amount of negative feedback taken respectively from the output and the first-order derivative of the output. The amount of the negative feedback that is taken from the first-order derivative of the output is denoted as 2α, whereas the amount of negative feedback that is taken directly from the output is denoted as ω_0^2. The response of this system is determined by the relative scale between α and ω_0 and four cases arise as detained in the following.

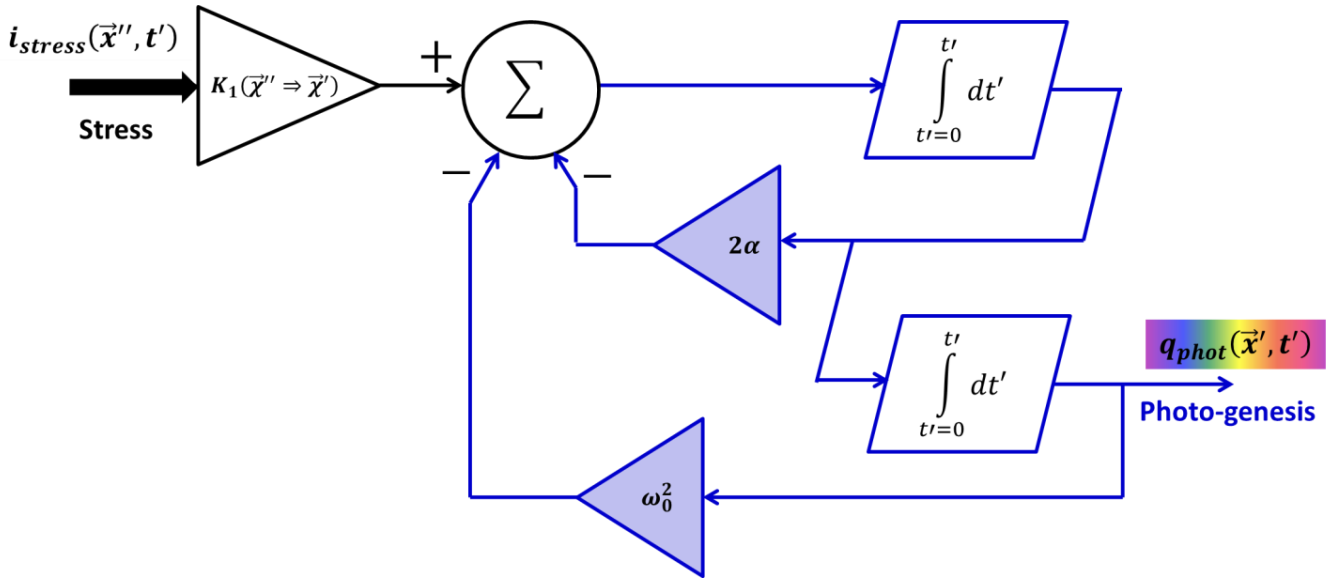

Figure 10. A stress-transfer pathway modeled to present a second-order low-pass response characterized by fixed kinetic rates.

4.6.1 The response corresponding to $\alpha = 0$ (un-damped response)

The transfer function is

$$\mathcal{H}_{stress}(\vec{\chi}'' \Rightarrow \vec{\chi}', s) = K_1(\vec{\chi}'' \Rightarrow \vec{\chi}') \cdot \frac{1}{s^2 + \omega_0^2} \quad (51)$$

that corresponds to an impulse response of

$$\hbar_{stress}(\vec{\chi}'' \Rightarrow \vec{\chi}', t') = K_{01}(\vec{\chi}'' \Rightarrow \vec{\chi}') \cdot \frac{1}{\omega_0} \cdot sin(\omega_0 t') \cdot u(t') \quad (52)$$

The response of this pathway to a bolus stress of magnitude A_{stress} represented by Eq. (23) is

$$q_{bolus}^{\alpha=0}(\vec{\chi}'' \Rightarrow \vec{\chi}', t') = A_{stress} \cdot K_{01}(\vec{\chi}'' \Rightarrow \vec{\chi}') \cdot \frac{1}{\omega_0} \cdot sin(\omega_0 t') \cdot u(t') \quad (53)$$

The response of this pathway to a step stress of magnitude A_{stress} represented by Eq. (25) is

$$q_{step}^{\alpha=0}(\vec{\chi}'' \Rightarrow \vec{\chi}', t') = A_{stress} \cdot K_{01}(\vec{\chi}'' \Rightarrow \vec{\chi}') \cdot \frac{1}{\omega_0^2} \cdot [1 - cos(\omega_0 t')] \cdot u(t') \quad (54)$$

4.6.2 The response corresponding to $0 < \alpha < \omega_0$ (under-damped response)

The transfer function is

$$\mathcal{H}_{stress}(\vec{\chi}'' \Rightarrow \vec{\chi}', s) = K_{01}(\vec{\chi}'' \Rightarrow \vec{\chi}') \cdot \frac{1}{(s+\alpha-j\omega_d)(s+\alpha+j\omega_d)} \quad (55)$$

The following notation is useful:

$$\omega_d = \sqrt{|\alpha^2 - \omega_0^2|} \quad (56)$$

Equation (55) corresponds to an impulse response of

$$\hbar_{stress}(\vec{\chi}'' \Rightarrow \vec{\chi}', t') = K_{01}(\vec{\chi}'' \Rightarrow \vec{\chi}') \cdot \frac{1}{\omega_d} \cdot e^{-\alpha t'} \cdot sin(\omega_d t') \cdot u(t') \quad (57)$$

The response of this pathway to a bolus stress of magnitude A_{stress} represented by Eq. (23) is

$$q_{bolus}^{\alpha<\omega_0}(\vec{\chi}'' \Rightarrow \vec{\chi}', t') = A_{stress} \cdot K_{01}(\vec{\chi}'' \Rightarrow \vec{\chi}') \cdot \frac{1}{\omega_d} \cdot e^{-\alpha t'} \cdot sin(\omega_d t') \cdot u(t') \quad (58)$$

The response of this pathway to a step stress of magnitude A_{stress} represented by Eq. (25) is

$$q_{step}^{\alpha<\omega_0}(\vec{\chi}'' \Rightarrow \vec{\chi}', t') = A_{stress} \cdot K_{01}(\vec{\chi}'' \Rightarrow \vec{\chi}') \cdot \frac{1}{\omega_d^2\left[1 + \left(\frac{\alpha}{\omega_d}\right)^2\right]} \left\{1 - \sqrt{1 + \left(\frac{\alpha}{\omega_d}\right)^2} \cdot e^{-\alpha t'} \cdot cos\left(\omega_d t' - tan^{-1}\left(\frac{\alpha}{\omega_d}\right)\right)\right\} \cdot u(t') \quad (59)$$

4.6.3 The response corresponding to $\alpha = \omega_0$ (critically damped response)

The transfer function is

$$\mathcal{H}_{stress}(\vec{\chi}'' \Rightarrow \vec{\chi}', s) = K_{01}(\vec{\chi}'' \Rightarrow \vec{\chi}') \cdot \frac{1}{(s+\alpha)^2} \quad (60)$$

That corresponds to an impulse response of

$$\hbar_{stress}(\vec{\chi}'' \Rightarrow \vec{\chi}', t') = K_{01}(\vec{\chi}'' \Rightarrow \vec{\chi}') \cdot t' \cdot e^{-\alpha t'} \cdot u(t') \quad (61)$$

The response of this pathway to a bolus stress of magnitude A_{stress} represented by Eq. (23) is

$$q_{bolus}^{\alpha=\omega_0}(\vec{\chi}'' \Rightarrow \vec{\chi}', t') = A_{stress} \cdot K_{01}(\vec{\chi}'' \Rightarrow \vec{\chi}') \cdot t' \cdot e^{-\alpha t'} \cdot u(t') \quad (62)$$

The response of this pathway to a step stress of magnitude A_{stress} represented by Eq. (25) is

$$q_{step}^{\alpha=\omega_0}(\vec{\chi}'' \Rightarrow \vec{\chi}', t') = A_{stress} \cdot K_{01}(\vec{\chi}'' \Rightarrow \vec{\chi}') \cdot \frac{1}{\alpha^2}\left[1 - e^{-\alpha t'}(1 + \alpha t')\right] \cdot u(t') \quad (63)$$

4.6.3 The response corresponding to $\alpha > \omega_0$ (over-damped response)

The transfer function is

$$\mathcal{H}_{stress}(\vec{\chi}'' \Rightarrow \vec{\chi}', s) = K_{01}(\vec{\chi}'' \Rightarrow \vec{\chi}') \cdot \frac{1}{(s+\alpha-\omega_d)(s+\alpha+\omega_d)} \quad (64)$$

That corresponds to an impulse response of

$$\hbar_{stress}(\vec{\chi}'' \Rightarrow \vec{\chi}', t') = K_{01}(\vec{\chi}'' \Rightarrow \vec{\chi}') \cdot \frac{1}{2\omega_d} \cdot e^{-(\alpha-\omega_d)t'} \cdot \left[1 - e^{-2\omega_d t'}\right] \cdot u(t') \quad (65)$$

The response of this pathway to a bolus stress of magnitude A_{stress} represented by Eq. (23) is

$$q_{bolus}^{\alpha>\omega_0}(\vec{\chi}'' \Rightarrow \vec{\chi}', t') = A_{stress} \cdot K_{01}(\vec{\chi}'' \Rightarrow \vec{\chi}') \cdot \frac{1}{2\omega_d} \cdot e^{-(\alpha-\omega_d)t'} \cdot \left[1 - e^{-2\omega_d t'}\right] \cdot u(t') \quad (66)$$

The response of this pathway to a step stress of magnitude A_{stress} represented by Eq. (25) is

$$q_{step}^{\alpha=\omega_0}(\vec{\chi}'' \Rightarrow \vec{\chi}', t') = A_{stress} \cdot K_{01}(\vec{\chi}'' \Rightarrow \vec{\chi}') \cdot \frac{1}{\alpha^2\left[1-\left(\frac{\omega_d}{\alpha}\right)^2\right]}$$
$$\cdot \left\{1 - \frac{1}{2\omega_d}\left[(\alpha+\omega_d)e^{-(\alpha-\omega_d)t'} - (\alpha-\omega_d)e^{-(\alpha+\omega_d)t'}\right]\right\} \cdot u(t') \quad (67)$$

4.7 Stress transfer characterized by one second-order band-pass response.

A stress-transfer pathway hypothesized to present a second-order band-pass response is illustrated in **Figure 11**. The system is similar to the one of Figure 10 in terms of the two kinetic rates determining the negative feedback taken respectively from the output and the first-order derivative of the output. The amount of the negative feedback that is taken from the first-order derivative of the output is denoted as 2α, whereas the amount of negative feedback that is taken directly from the output is denoted as ω_0^2. The system differs from that of Figure 10 in terms of how the input is passed through to the output, as it has the first-order derivative of the input passed to the output instead of the input itself. The response of this system is also determined by the relative scale between α and ω_0 and four cases arise as detained in the following, by using the same definition of ω_d of Eq. (56).

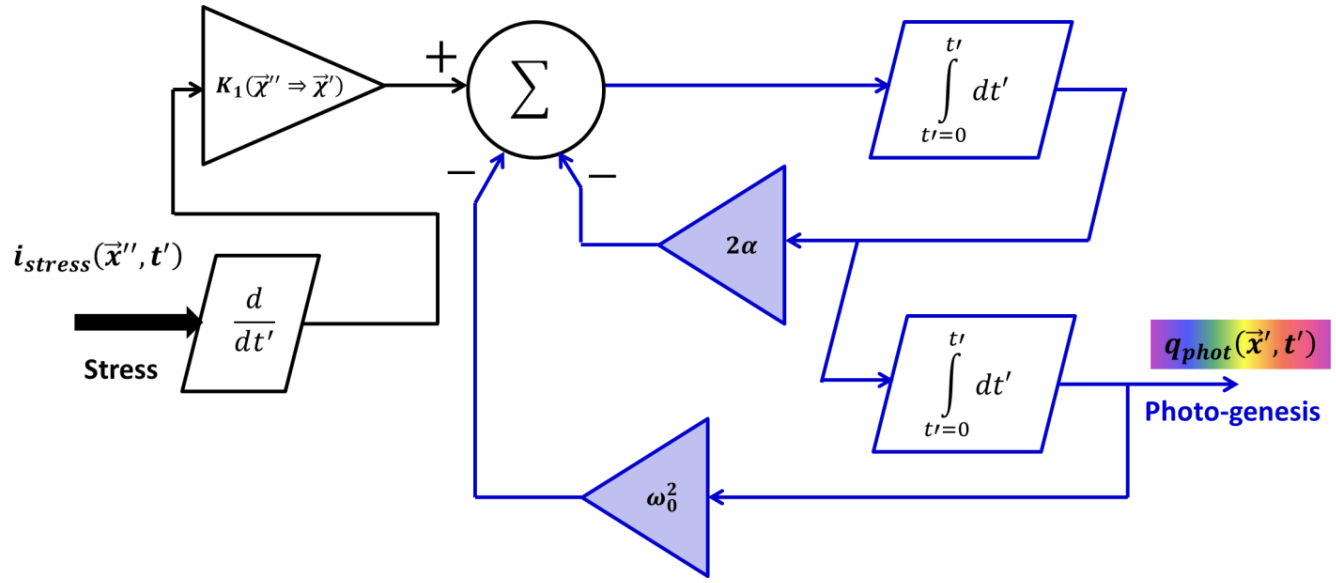

Figure 11 A stress-transfer pathway modeled to present a second-order band-pass response characterized by fixed kinetic rates.

4.7.1 The response corresponding to $\alpha = 0$ (un-damped response)

The transfer function of the pathway is

$$\mathcal{H}_{stress}(\vec{\chi}'' \Rightarrow \vec{\chi}', s) = K_{01}(\vec{\chi}'' \Rightarrow \vec{\chi}') \cdot \frac{s}{s^2+\omega_0^2} \quad (68)$$

The corresponding impulse response is

$$\hbar_{stress}(\vec{\chi}'' \Rightarrow \vec{\chi}', t') = A_{stress} \cdot K_{01}(\vec{\chi}'' \Rightarrow \vec{\chi}') \cdot cos(\omega_0 t') \cdot u(t') \quad (69)$$

The response of this pathway to a bolus stress of magnitude A_{stress} represented by Eq. (23) is

$$q_{step}^{\alpha=0}(\vec{\chi}'' \Rightarrow \vec{\chi}', t') = A_{stress} \cdot K_{01}(\vec{\chi}'' \Rightarrow \vec{\chi}') \cdot cos(\omega_0 t') \cdot u(t') \quad (70)$$

The response of this pathway to a step stress of magnitude A_{stress} represented by Eq. (25) is

$$q_{step}^{\alpha=0}(\vec{\chi}'' \Rightarrow \vec{\chi}', t') = A_{stress} \cdot K_{01}(\vec{\chi}'' \Rightarrow \vec{\chi}') \cdot \frac{1}{\omega_0} \cdot sin(\omega_0 t') \cdot u(t') \quad (71)$$

4.7.2 The response corresponding to $0 < \alpha < \omega_0$ (under-damped response)

The transfer function of the pathway is

$$\mathcal{H}_{stress}(\vec{\chi}'' \Rightarrow \vec{\chi}', s) = K_{01}(\vec{\chi}'' \Rightarrow \vec{\chi}') \cdot \frac{s}{(s+\alpha-j\omega_d)(s+\alpha+j\omega_d)} \quad (72)$$

The corresponding impulse response is

$$\hbar_{stress}(\vec{\chi}'' \Rightarrow \vec{\chi}', t') = K_{01}(\vec{\chi}'' \Rightarrow \vec{\chi}') \cdot \sqrt{1+\left(\frac{\alpha}{\omega_d}\right)^2} \cdot e^{-\alpha t'} \cdot cos\left[\omega_d t' - tan^{-1}\left(\frac{\alpha}{\omega_d}\right)\right] \cdot u(t') \quad (73)$$

The response of this pathway to a bolus stress of magnitude A_{stress} represented by Eq. (23) is

$$q_{bolus}^{\alpha<\omega_0}(\vec{\chi}'' \Rightarrow \vec{\chi}', t') = A_{stress} \cdot K_{01}(\vec{\chi}'' \Rightarrow \vec{\chi}') \cdot \sqrt{1+\left(\frac{\alpha}{\omega_d}\right)^2} \cdot e^{-\alpha t'} \cdot cos\left[\omega_d t' - tan^{-1}\left(\frac{\alpha}{\omega_d}\right)\right] \cdot u(t') \quad (75)$$

The response of this pathway to a step stress of magnitude A_{stress} represented by Eq. (25) is

$$q_{step}^{\alpha<\omega_0}(\vec{\chi}'' \Rightarrow \vec{\chi}', t') = A_{stress} \cdot K_{01}(\vec{\chi}'' \Rightarrow \vec{\chi}') \cdot \frac{1}{\omega_d} \cdot e^{-\alpha t'} \cdot sin(\omega_d t') \cdot u(t') \quad (76)$$

4.7.3 The response corresponding to $\alpha = \omega_0$ (critically-damped response)

The transfer function of the pathway is

$$\mathcal{H}_{stress}(\vec{\chi}'' \Rightarrow \vec{\chi}', s) = K_{01}(\vec{\chi}'' \Rightarrow \vec{\chi}') \cdot \frac{s}{(s+\alpha)^2} \quad (77)$$

The corresponding impulse response is

$$\hbar_{stress}(\vec{\chi}'' \Rightarrow \vec{\chi}', t') = K_{01}(\vec{\chi}'' \Rightarrow \vec{\chi}') \cdot e^{-\alpha t'} \cdot (1-\alpha t') \cdot u(t') \quad (78)$$

The response of this pathway to a bolus stress of magnitude A_{stress} represented by Eq. (23) is

$$q_{bolus}^{\alpha=\omega_0}(\vec{\chi}'' \Rightarrow \vec{\chi}', t') = A_{stress} \cdot K_{01}(\vec{\chi}'' \Rightarrow \vec{\chi}') \cdot e^{-\alpha t'} \cdot (1-\alpha t') \cdot u(t') \quad (79)$$

The response of this pathway to a step stress of magnitude A_{stress} represented by Eq. (25) is

$$q_{step}^{\alpha=\omega_0}(\vec{\chi}'' \Rightarrow \vec{\chi}', t') = A_{stress} \cdot K_{01}(\vec{\chi}'' \Rightarrow \vec{\chi}') \cdot t' \cdot e^{-\alpha t'} \cdot u(t') \quad (80)$$

4.7.4 The response corresponding to $\alpha > \omega_0$ (over-damped response)

The transfer function of the pathway is

$$\mathcal{H}_{stress}(\vec{\chi}'' \Rightarrow \vec{\chi}', s) = K_{01}(\vec{\chi}'' \Rightarrow \vec{\chi}') \cdot \frac{s}{(s+\alpha-\omega_d)(s+\alpha+\omega_d)} \quad (81)$$

The corresponding impulse response is

$$\hbar_{stress}(\vec{\chi}'' \Rightarrow \vec{\chi}', t') = K_{01}(\vec{\chi}'' \Rightarrow \vec{\chi}') \cdot \frac{1}{2\omega_d} \cdot \left[(\alpha+\omega_d)e^{-(\alpha+\omega_d)t'} - (\alpha-\omega_d)e^{-(\alpha-\omega_d)t'}\right] \cdot u(t') \quad (82)$$

The response of this pathway to a bolus stress of magnitude A_{stress} represented by Eq. (23) is

$$q_{bolus}^{\alpha>\omega_0}(\vec{\chi}'' \Rightarrow \vec{\chi}', t') = A_{stress} \cdot K_{01}(\vec{\chi}'' \Rightarrow \vec{\chi}') \cdot \frac{1}{2\omega_d} \cdot \left[(\alpha+\omega_d)e^{-(\alpha+\omega_d)t'} - (\alpha-\omega_d)e^{-(\alpha-\omega_d)t'}\right] \cdot u(t') \quad (83)$$

The response of this pathway to a step stress of magnitude A_{stress} represented by Eq. (25) is

$$q_{step}^{\alpha>\omega_0}(\vec{\chi}'' \Rightarrow \vec{\chi}', t') = A_{stress} \cdot K_{01}(\vec{\chi}'' \Rightarrow \vec{\chi}') \cdot \frac{1}{2\omega_d} \cdot e^{-(\alpha-\omega_d)t'} \cdot \left[1 - e^{-2\omega_d t'}\right] \cdot u(t') \quad (84)$$

5. Numerical evaluations of the responses of the stress-transfer pathways to bolus and step inputs

This section numerically assesses the responses of the hypothesized stress-transfer pathways to a bolus input and a step input. To facilitate the numerical assessment, the responses of the stress-transfer pathways to a bolus input are grouped in **Table 2** and those to a step input are grouped in **Table 3**. Both tables contain three sub-tables. The sub-table 1 compares the responses of the stress-transfer pathways hypothesized to consist of first-order low-pass systems with fixed kinetic rates or a time-varying kinetic rate. The sub-table 2 compares the responses of the stress-transfer pathways hypothesized to reveal second-order low-pass characteristics with fixed kinetic rates but differing in the damping. The sub-table 3

compares the responses of the stress-transfer pathways hypothesized to reveal second-order band-pass characteristics with fixed kinetic rates but differing in damping.

The equations included in Table 2 and 3 are implemented according to the following principles: (1) The kinetics is evaluated over a time scale of [0 1] with a temporal resolution of 10^{-4}. This resolution corresponds to measuring 10,000 times over the duration of the acquisition or covering a total of 4 orders of magnitude in time. This relative scaling is applicable to the decay kinetics of delayed UPE because what is presented is the rate of the intensity change over time, and that is always affected by the temporal resolution of the measurement and the total duration of the data acquisition. (2) $K_{01} = 1$ is assigned for all systems presenting first-order low-pass responses. (3) A total of 7 stages are configured for the stress-transfer pathway hypothesized to reveal three or more in-parallel first-order low-pass responses. This follows a report that the kinetics of the delayed UPE in response to photo-illumination is fitted by a total of 4 or 7 exponential functions [34]. (3) The kinetic rate of the single first-order low-pass system is set as $K_{1\Omega} = 10$, or 10 times in magnitude of the total duration of evaluation. This is equivalent to have the time-constant of the single first-order low-pass system that is 10^{-1} of the total duration of evaluation. (4) For systems containing two or more first-order low-pass responses determined by fixed kinetic rates, the kinetic rate of the first stage of the multiple-exponential system is set as $K_{\mathrm{M}\Omega} = 10$, i.e. 10 times in magnitude of the total duration of evaluation. The kinetic rates of the other pathways of $m \in [1, M-1]$ are defined as $K_{m\Omega}$=$K_{M\Omega} \cdot exp(1-m)$. This exponential decrease of the kinetic rates of the rest of the pathways is equivalent to having the time-constants of the rest of pathways to increase at an exponential rate. (4) For the system revealing first-order low-pass response associated with a time-varying kinetic rate, the terminal kinetic rate of the system at the beginning of the duration of evaluation is set as $K_{1\Omega}(0) = 10$, i.e. 10 times in magnitude of the total duration of evaluation. The kinetic rates of the later instant is defined as $K_{1\Omega}(t)$=$K_{1\Omega}(0) \cdot exp[-K_{\mathrm{v}} \cdot t]$, where $K_{\mathrm{v}} = 50$. This makes the kinetic rate of the hypothesized pathway to decrease exponentially or equivalently the response of the pathway to slow down at an exponential rate. (5) For the systems revealing second-order responses, zero-damping responses are not evaluated because it is simply the limiting case of under-damped response. The underdamped responses are evaluated at $\alpha = 10^{-1}\omega_0$ and $\alpha = 2^{-1}\omega_0$. The overdamped responses are evaluated at $\alpha = 2\omega_0$ and $\alpha = 10\omega_0$. The critically damped response is evaluated. $\omega_0 = 100$ is assigned to all cases.

Table 2 The response of the hypothesized stress-transfer pathways to a bolus input of an intensity of A_{stress}

2.1 Stress-transfer pathway that reveals first-order low-pass kinetics with a fixed or time-varying time constant

Stress-transfer pathway	**response**
Single first-order low pass	$q^{1}_{bolus}(\vec{\chi}',t') = [A_{stress}\cdot\delta(\vec{\chi}-\vec{\chi}'')\cdot K_{01}(\vec{\chi}''\Rightarrow\vec{\chi}')\cdot K_{1\upsilon}(\vec{\chi}')]\cdot e^{-K_{1\upsilon}(\vec{\chi}')\cdot t'}\cdot u(t')$ (38)
Double first order low pass	$q^{2}_{bolus}(\vec{\chi}',t') = A_{stress}\cdot\delta(\vec{\chi}-\vec{\chi}'')\cdot\sum_{m=1}^{2}\left[K_{0m}(\vec{\chi}''\Rightarrow\vec{\chi}')\cdot K_{m\upsilon}(\vec{\chi}')\cdot e^{-K_{m\upsilon}(\vec{\chi}')\cdot t'}\right]\cdot u(t')$ (42)
Multi first order low pass	$q^{M}_{bolus}(\vec{\chi}',t') = A_{stress}\cdot\delta(\vec{\chi}-\vec{\chi}'')\cdot\sum_{m=1}^{M}\left[K_{0m}(\vec{\chi}''\Rightarrow\vec{\chi}')\cdot K_{m\upsilon}(\vec{\chi}')\cdot e^{-K_{m\upsilon}(\vec{\chi}')\cdot t'}\right]\cdot u(t')$ (46)
Single first order low pass with varying time constant	$q^{\tau(t')}_{bolus}(\vec{\chi}',t') = [A_{stress}\cdot\delta(\vec{\chi}-\vec{\chi}'')\cdot K_{01}(\vec{\chi}''\Rightarrow\vec{\chi}')\cdot K_{1\upsilon}(\vec{\chi}')]\cdot e^{-K_{1\upsilon}(\vec{\chi}',t')\cdot t'}\cdot u(t')$ (49)

2.2 Stress-transfer pathway that reveals second-order low-pass kinetics with varying damping factors

Stress-transfer pathway	**response**
$\boldsymbol{\alpha = 0}$	$q^{\alpha=0}_{bolus}(\vec{\chi}''\Rightarrow\vec{\chi}',t') = A_{stress}\cdot K_{01}(\vec{\chi}''\Rightarrow\vec{\chi}')\cdot\frac{1}{\omega_0}\cdot sin(\omega_0 t')\cdot u(t')$ (53)
$\boldsymbol{0 < \alpha < \omega_0}$	$q^{\alpha<\omega_0}_{bolus}(\vec{\chi}''\Rightarrow\vec{\chi}',t') = A_{stress}\cdot K_{01}(\vec{\chi}''\Rightarrow\vec{\chi}')\cdot\frac{1}{\omega_d}\cdot e^{-\alpha t'}\cdot sin(\omega_d t')\cdot u(t')$ (58)
$\boldsymbol{\alpha = \omega_0}$	$q^{\alpha=\omega_0}_{bolus}(\vec{\chi}''\Rightarrow\vec{\chi}',t') = A_{stress}\cdot K_{01}(\vec{\chi}''\Rightarrow\vec{\chi}')\cdot t'\cdot e^{-\alpha t'}\cdot u(t')$ (62)
$\boldsymbol{\alpha > \omega_0}$	$q^{\alpha>\omega_0}_{bolus}(\vec{\chi}''\Rightarrow\vec{\chi}',t') = A_{stress}\cdot K_{01}(\vec{\chi}''\Rightarrow\vec{\chi}')\cdot\frac{1}{2\omega_d}\cdot e^{-(\alpha-\omega_d)t'}\cdot\left[1-e^{-2\omega_d t'}\right]\cdot u(t')$ (66)

2.3 Stress-transfer pathway that reveals second-order band-pass kinetics with varying damping factors

Stress-transfer pathway	**Response**
$\boldsymbol{\alpha = 0}$	$q_{step}^{\alpha=0}(\vec{\chi}'' \Rightarrow \vec{\chi}', t') = A_{stress} \cdot K_{01}(\vec{\chi}'' \Rightarrow \vec{\chi}') \cdot cos(\omega_0 t') \cdot u(t')$ (70)
$\boldsymbol{0 < \alpha < \omega_0}$	$q_{bolus}^{\alpha<\omega_0}(\vec{\chi}'' \Rightarrow \vec{\chi}', t') = A_{stress} \cdot K_{01}(\vec{\chi}'' \Rightarrow \vec{\chi}') \cdot \sqrt{1 + \left(\frac{\alpha}{\omega_d}\right)^2} \cdot e^{-\alpha t'} \cdot cos\left[\omega_d t' - tan^{-1}\left(\frac{\alpha}{\omega_d}\right)\right] \cdot u(t')$ (75)
$\boldsymbol{\alpha = \omega_0}$	$q_{bolus}^{\alpha=\omega_0}(\vec{\chi}'' \Rightarrow \vec{\chi}', t') = A_{stress} \cdot K_{01}(\vec{\chi}'' \Rightarrow \vec{\chi}') \cdot e^{-\alpha t'} \cdot (1 - \alpha t') \cdot u(t')$ (79)
$\boldsymbol{\alpha > \omega_0}$	$q_{bolus}^{\alpha>\omega_0}(\vec{\chi}'' \Rightarrow \vec{\chi}', t') = A_{stress} \cdot K_{01}(\vec{\chi}'' \Rightarrow \vec{\chi}') \cdot \frac{1}{2\omega_d} \cdot \left[(\alpha + \omega_d)e^{-(\alpha+\omega_d)t'} - (\alpha - \omega_d)e^{-(\alpha-\omega_d)t'}\right] \cdot u(t')$ (83)

Table 3 The response of the hypothesized stress-transfer pathways to a step input of an intensity of A_{stress}

3.1 Stress-transfer pathway that reveals first-order low-pass kinetics with a fixed or time-varying time constant

Stress-transfer pathway	**response**
Single first-order low pass	$q_{step}^{1}(\vec{\chi}', t') = [A_{stress} \cdot \delta(\vec{\chi} - \vec{\chi}'') \cdot K_{01}(\vec{\chi}'' \Rightarrow \vec{\chi}')] \cdot \left[1 - e^{-K_{1\mho}(\vec{\chi}') \cdot t'}\right] u(t')$ (39)
Double first order low pass	$q_{bolus}^{2}(\vec{\chi}', t') = A_{stress} \cdot \delta(\vec{\chi} - \vec{\chi}'') \cdot \sum_{m=1}^{2}\left\{K_{0m}(\vec{\chi}'' \Rightarrow \vec{\chi}') \cdot \left[1 - e^{-K_{m\mho}(\vec{\chi}') \cdot t'}\right]\right\} u(t')$ (43)
Multi first order low pass	$q_{step}^{M}(\vec{\chi}', t') = A_{stress} \cdot \delta(\vec{\chi} - \vec{\chi}'') \cdot \sum_{m=1}^{M}\left\{K_{0m}(\vec{\chi}'' \Rightarrow \vec{\chi}') \cdot \left[1 - e^{-K_{m\mho}(\vec{\chi}') \cdot t'}\right]\right\} u(t')$ (47)
Single first order low pass with varying time constant	$q_{step}^{\tau(t')}(\vec{\chi}', t') = [A_{stress} \cdot \delta(\vec{\chi} - \vec{\chi}'') \cdot K_{01}(\vec{\chi}'' \Rightarrow \vec{\chi}')] \cdot \left[1 - e^{-K_{1\mho}(\vec{\chi}', t') \cdot t'}\right] u(t')$ (50)

3.2 Stress-transfer pathway that reveals second-order low-pass kinetics with varying damping factors

Stress-transfer pathway	**response**
$\boldsymbol{\alpha = 0}$	$q_{step}^{\alpha=0}(\vec{\chi}'' \Rightarrow \vec{\chi}', t') = A_{stress} \cdot K_{01}(\vec{\chi}'' \Rightarrow \vec{\chi}') \cdot \frac{1}{\omega_0^2} \cdot [1 - cos(\omega_0 t')] \cdot u(t')$ (54)
$\boldsymbol{0 < \alpha < \omega_0}$	$q_{step}^{\alpha<\omega_0}(\vec{\chi}'' \Rightarrow \vec{\chi}', t') = A_{stress} \cdot K_{01}(\vec{\chi}'' \Rightarrow \vec{\chi}') \cdot \frac{1}{\omega_d^2 \left[1 + \left(\frac{\alpha}{\omega_d}\right)^2\right]}$ $\left\{1 - \sqrt{1 + \left(\frac{\alpha}{\omega_d}\right)^2} \cdot e^{-\alpha t'} \cdot cos\left(\omega_d t' - tan^{-1}\left(\frac{\alpha}{\omega_d}\right)\right)\right\} \cdot u(t')$ (59)
$\boldsymbol{\alpha = \omega_0}$	$q_{step}^{\alpha=\omega_0}(\vec{\chi}'' \Rightarrow \vec{\chi}', t') = A_{stress} \cdot K_{01}(\vec{\chi}'' \Rightarrow \vec{\chi}') \cdot \frac{1}{\alpha^2}\left[1 - e^{-\alpha t'}(1 + \alpha t')\right] \cdot u(t')$ (63)
$\boldsymbol{\alpha > \omega_0}$	$q_{step}^{\alpha=\omega_0}(\vec{\chi}'' \Rightarrow \vec{\chi}', t') = A_{stress} \cdot K_{01}(\vec{\chi}'' \Rightarrow \vec{\chi}') \cdot \frac{1}{\alpha^2 \left[1 - \left(\frac{\omega_d}{\alpha}\right)^2\right]}$ $\cdot \left\{1 - \frac{1}{2\omega_d}\left[(\alpha + \omega_d)e^{-(\alpha-\omega_d)t'} - (\alpha - \omega_d)e^{-(\alpha+\omega_d)t'}\right]\right\} \cdot u(t')$ (67)

3.3 Stress-transfer pathway that reveals second-order band-pass kinetics with varying damping factors

Stress-transfer pathway	**response**	
$\boldsymbol{\alpha = 0}$	$q_{step}^{\alpha=0}(\vec{\chi}'' \Rightarrow \vec{\chi}', t') = A_{stress} \cdot K_{01}(\vec{\chi}'' \Rightarrow \vec{\chi}') \cdot \frac{1}{\omega_0} \cdot sin(\omega_0 t') \cdot u(t')$	(71)
$\boldsymbol{0 < \alpha < \omega_0}$	$q_{step}^{\alpha<\omega_0}(\vec{\chi}'' \Rightarrow \vec{\chi}', t') = A_{stress} \cdot K_{01}(\vec{\chi}'' \Rightarrow \vec{\chi}') \cdot \frac{1}{\omega_d} \cdot e^{-\alpha t'} \cdot sin(\omega_d t') \cdot u(t')$	(76)
$\boldsymbol{\alpha = \omega_0}$	$q_{step}^{\alpha=\omega_0}(\vec{\chi}'' \Rightarrow \vec{\chi}', t') = A_{stress} \cdot K_{01}(\vec{\chi}'' \Rightarrow \vec{\chi}') \cdot t' \cdot e^{-\alpha t'} \cdot u(t')$	(80)
$\boldsymbol{\alpha > \omega_0}$	$q_{step}^{\alpha>\omega_0}(\vec{\chi}'' \Rightarrow \vec{\chi}', t') = A_{stress} \cdot K_{01}(\vec{\chi}'' \Rightarrow \vec{\chi}') \cdot \frac{1}{2\omega_d} \cdot e^{-(\alpha-\omega_d)t'} \cdot \left[1 - e^{-2\omega_d t'}\right] \cdot u(t')$	(84)

5.1 The responses of the hypothesized stress-transfer pathways to a bolus input

The responses of the hypothesized stress-transfer pathways to bolus input as summarized in Table 2 are displayed in **Figure 12**, for the selected configurations of the variables involved.

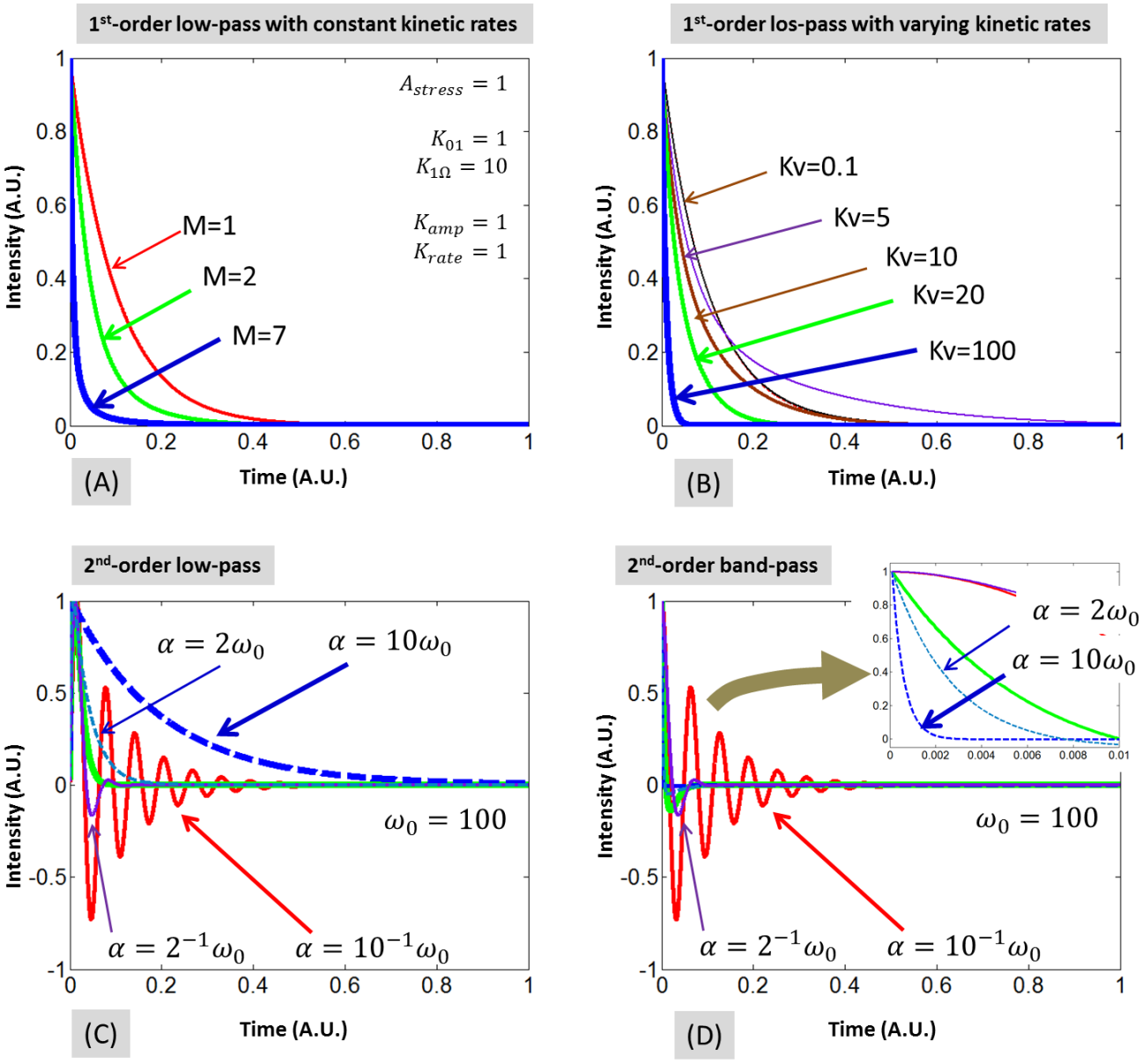

Figure 12 The responses of the hypothesized stress-transfer pathways to a bolus input. (A) The responses characterized by single or multiple in-parallel first-order low-pass systems with constant kinetic rates. (B) The responses characterized by single first-order low-pass system with slowly varying kinetic rate. (C) The responses characterized by a second-order low-pass system with fixed kinetic rates but different non-zero damping factors. (D) The responses characterized by a second-order band-pass system with fixed kinetic rates but different non-zero damping factors.

The (A) specifies the bolus responses of the stress-transfer pathways characterized by single or multiple in-parallel first-order low-pass systems having constant kinetic rates. The "*M*" number indicates the number of first-order low-pass system hypothesized to be involved in the stress-transfer pathway. M=1

corresponds to a kinetic decay defined by a single exponential function. M=2 corresponds to a kinetic decay defined by a combination of two exponential functions. According to Eq. (42), the ratio of the initial intensities of these two exponential functions is identical to the ratio of the kinetic rates of the two exponential functions. M=7 corresponds to a kinetic decay defined by a combination of seven exponential functions. The initial intensities and the kinetic rates of these exponential functions decrease exponentially according to the aforementioned principles. As the number of exponential functions increase, the decay pattern deviates more and more from the single-exponential curve. The initial decay becomes faster and the tail grounds at much slower rate. The transition between the fast initial decay and the slow later lag is more pronounced as the number of the first-order low-pass pathways increase.

The (B) is specific to the bolus responses of the stress-transfer pathways characterized by single first-order low-pass systems with a time-varying kinetic rate. The kinetic rate decreases exponentially according to the aforementioned principles. The decay pattern corresponding to Kv=0.1, which slows down the kinetic rate by 9.5% over the course of the duration is indistinguishable from the pattern of single first-order low-pass response defined by a fixed kinetic rate identical to the initial value of the kinetic rate of this system with a time-varying kinetics. As the kinetic rate varies faster, the decay pattern deviates more and more from the single-exponential curve. The initial decay becomes faster and the grounding tail becomes longer. The transition between the fast initial decay and the slow later lag is more pronounced as the rate of change of the kinetic constant increases.

The (C) is specific to the bolus responses of the stress-transfer pathways characterized by a second-order low-pass systems with constant kinetic rates but with different non-zero damping factors. The under-damped responses evaluated at $\alpha = \frac{1}{10}\omega_0$ has multiple periods of oscillations enveloped by an exponential decay function. The under-damped response evaluated at $\alpha = \frac{1}{2}\omega_0$ presents oscillatory pattern that quickly decays to zero. The over-damped response evaluated at $\alpha = 10\omega_0$ decays at a rate slower than the single first-order low-pass system shown in (A). The over-damped responses evaluated at $\alpha = 2\omega_0$ decays at a rate faster than the single first-order low-pass system and the dual in-parallel first-order low-pass system shown in (A). The critically-damped response resembles the one of (A) that corresponds to the combination of 7 in-parallel first-order low-pass responses.

The (D) is specific to the bolus responses of the stress-transfer pathways characterized by a second-order band-pass systems with constant kinetic rates but with different non-zero damping factors. The under-damped response evaluated at $\alpha = \frac{1}{10}\omega_0$ has multiple periods of oscillations enveloped by an exponential decay function. The under-damped response evaluated at $\alpha = \frac{1}{2}\omega_0$ presented oscillatory pattern that quickly decays to zero. The over-damped responses evaluated at both $\alpha = 10\omega_0$ and $\alpha = 2\omega_0$ decay much faster than those in (C). The critically-damped response also decays mush faster than the one of (A) that corresponds to the combination of 7 in-parallel first-order low-pass responses. The decay patterns over the first 1% of the duration are displayed in the inset figure. The over-damped response evaluated at $\alpha = 2\omega_0$ decays at a rate faster than $\alpha = 10\omega_0$, which is faster than the critically damped response.

5.2 The responses of the hypothesized stress-transfer pathways to a step input

The responses of the hypothesized stress-transfer pathways to step input as summarized in Table 2 are displayed in **Figure 13**, for the selected configurations of the variables involved.

The (A) specifies the step responses of the stress-transfer pathways characterized by single or multiple in-parallel first-order low-pass systems having constant kinetic rates. The "M" number indicates the number of first-order low-pass system hypothesized to be involved in the stress-transfer pathway. M=1 corresponds to a kinetic change defined by a single exponential function. M=2 corresponds to a kinetic change defined by a combination of two exponential functions. M=7 corresponds to a kinetic change

defined by a combination of seven exponential functions. The kinetic rates of these exponential functions decrease exponentially according to the aforementioned principles. As the number of exponential functions increase, the uprising pattern deviates more and more from the single-exponential curve. The initial increase becomes faster and the saturating tail becomes longer. The transition between the fast initial increase and the slow later saturating tail is more pronounced as the number of the first-order low-pass pathways increase.

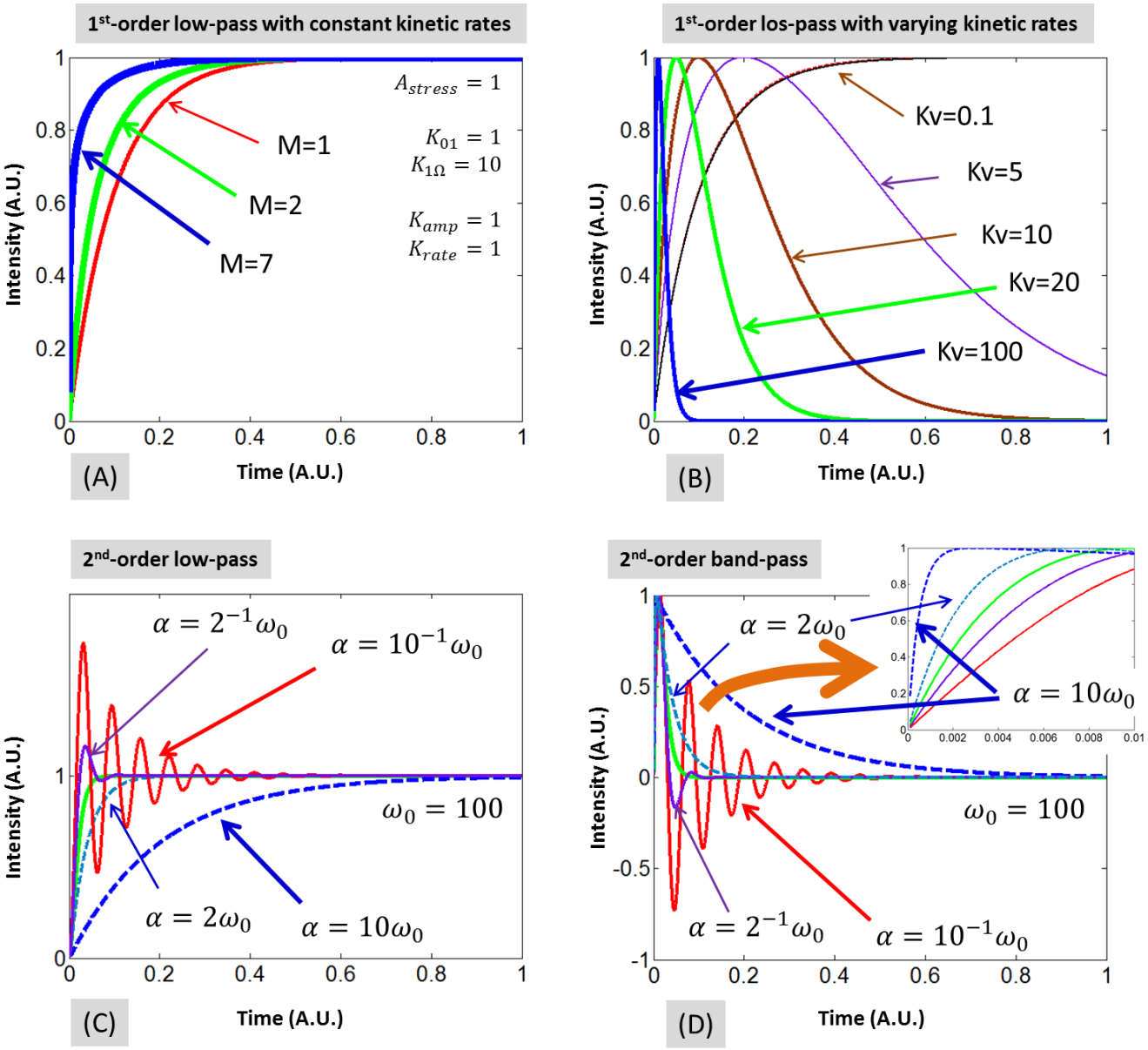

Figure 13 The responses of the hypothesized stress-transfer pathways to a step input. (A) The responses characterized by single or multiple in-parallel first-order low-pass systems with constant kinetic rates. (B) The responses characterized by single first-order low-pass system with slowly varying kinetic rate. (C) The responses characterized by a second-order low-pass system with fixed kinetic rates but different non-zero damping factors. (D) The responses characterized by a second-order band-pass system with fixed kinetic rates but different non-zero damping factors.

The (B) is specific to the step responses of the stress-transfer pathways characterized by single first-order low-pass systems with a time-varying kinetic rate. The kinetic rate decreases exponentially according to the aforementioned principles. The step-response pattern for Kv=0.1, which slows down the kinetic rate by 9.5% over the course of the duration is indistinguishable from the pattern of single first-order low-pass response defined by a fixed kinetic rate identical to the initial value of the kinetic rate of this system with a time-varying kinetics. As the kinetic rate varies faster, the step-response pattern deviates more and more from the single-exponential curve. The initial uprising becomes faster that is followed by the peaking of the value and a later decay that grounds as the time increases. The decaying pattern following the peak becomes increasingly like a hyperbolic pattern as the rate of change of the kinetic constant increases. The bi-phasic pattern is also more pronounced as the rate of change of the kinetic constant increases.

The (C) is specific to the step responses of the stress-transfer pathways characterized by a second-order low-pass systems with constant kinetic rates but with different non-zero damping factors. The under-damped response evaluated at $\alpha = \frac{1}{10}\omega_0$ has multiple periods of oscillations enveloped by an exponential decay function to stabilize to a steady-state of 1. The under-damped response evaluated at $\alpha = \frac{1}{2}\omega_0$ presents oscillatory pattern that quickly stabilizes to a steady-state of 1. The over-damped response evaluated at $\alpha = 10\omega_0$ increases to the steady-state value of 1 at a rate slower than the single first-order low-pass system shown in (A). The over-damped responses evaluated at $\alpha = 2\omega_0$ increases to the steady-state value of 1 at a rate faster than the single first-order low-pass system and the dual in-parallel first-order low-pass system shown in (A). The critically-damped response resembles the one of (A) that corresponds to the combination of 7 in-parallel first-order low-pass responses.

The (D) is specific to the step responses of the stress-transfer pathways characterized by a second-order band-pass systems with constant kinetic rates but with different non-zero damping factors. The under-damped response evaluated at $\alpha = \frac{1}{10}\omega_0$ has multiple periods of oscillations enveloped by an exponential decay function that stabilizes to zero. The under-damped response evaluated at $\alpha = \frac{1}{2}\omega_0$ presented oscillatory pattern that quickly decays to zero. The over-damped responses evaluated at both $\alpha = 10\omega_0$ and $\alpha = 2\omega_0$ peak sharply then decay to zero, with the rate of the decay faster in $\alpha = 2\omega_0$ than in $\alpha = 10\omega_0$. The critically-damped response decays after a sharp uprising at a pattern similar to the one of (A) of Figure 12 that corresponds to the bolus response of the combination of 7 in-parallel first-order low-pass responses. The changes of the five cases over the first 1% of the duration are displayed in the inset figure. The over-damped response evaluated at $\alpha = 2\omega_0$ increases slower than $\alpha = 10\omega_0$, which is faster than the critically damped response.

6. Discussions:

The commonly reported spontaneous biophoton emission intensity is 100s of photons per second per square centimeter [9, 27, 108-110]. At the visible wavelength of 500nm, a photon count rate of 100 photons per second per square centimeter corresponds to an irradiance of $3.98 \times 10^{-17} W \cdot cm^{-2}$ or $\sim 0.04 fW \cdot cm^{-2}$. This irradiance is comparable to the photon fluence rate measured at 10cm from a source of 1μW power in an unbounded homogeneous tissue medium having an absorption coefficient of $0.106 cm^{-1}$ and a reduced scattering coefficient of $10 cm^{-1}$. Even methods like impedance matching can be used to enhance the light transmission from the tissue to the detection window of photo-detector, the intensity of spontaneous UPE is weak. The extremely small intensity of spontaneous biophoton emission has hindered the mechanism exploration beyond the known association of biophoton emission with the oxidative stress [111].

There is a lasting dichotomy in the interests on spontaneous ultra-weak photon emissions from organisms known to associate with metabolic activities. On one hand, the ultra-weak level of photons

emitted as spontaneous UPE challenges the sensitivity and specificity of mechanistic discovery of oxidative metabolism, because the signal is too long to acquire and too weak to utilize. On the other hand, the lack of mechanistic understanding limits the development of more efficient experimental methods for enhancing the signal-to-noise ratio of detecting UPE. The enhancement of UPE photon counts by delayed UPE following exogenous stress or stimulation clearly renders the means for applying external control to modulate the homeostasis to probe the oxidative metabolism. However, major questions arise that include how to optimize the control to maximize the photon count in association with a specific external stress, how to identify the number of metabolic pathways involved in the production of the photons emitted as delayed UPE, and what physiological mechanisms underline the exact metabolic pathways. None of these questions could be answered without accurate and robust understandings of the kinetics of delayed UPE, because all information of the metabolic response that reveals delayed UPE can be exploited only by using the kinetics of delayed UPE, when the external stimulation can be modulated.

As were summarized from approximately 66 reports of delayed UEP phenomena in Section 2, the kinetic patterns of delayed UPE do not appear to be simple. The hyperbolic decay pattern is the one that was understood the most; however the hyperbolic decaying pattern is applicable to just less than 35% of the reports surveyed. For the rest of the delayed UPE phenomena, there are more single-exponential cases than the patterns setting between the single-exponential and the hyperbolic ones. The patterns that set between the single-exponential and the hyperbolic ones are accountable by using two or more exponential functions. Note that the hyperbolic function fitting the delayed UPE kinetics appear as a compressed form, and a compressed hyperbolic function can in principle be decomposed to the summation of an infinite number of exponential functions [107] through a Laplace transform approach. In such decomposition, the coefficient of each exponential function with negative argument corresponds to a probability distribution of the kinetic rate of the negative argument. Therefore a hyperbolic function is essentially a combination of many exponential functions that decay. Since each exponential component of negative argument constitutes a first-order low-pass response, a lesser amount of exponential functions contributing to the decay kinetics will make the kinetics decay look more like a pure exponential decay. Conversely, the involvement of more individually pure exponential kinetics can make the composite kinetics pattern deviate more from a pure exponential pattern and more like a hyperbolic pattern. That is the case shown in Figure 12(A) for the response to a bolus input by the stress-transfer pathways hypothesized to consist of one, two, and seven exponential functions.

It is noted that, the decomposition of a hyperbolic function to exponential functions is mechanistically similar to Fourier series expansion of a periodical function. It is thus straightforward to stipulate that the most dominant kinetic component of the decomposition of the hyperbolic function will be the one that varies the fastest thus has the highest kinetic energy with it, just like the fundamental-frequency component of a Fourier series expansion. And the kinetic component that varies slower should have a smaller kinetic energy with it. That is the principle used to set the initial values of the individual single-exponential components of the stress-transfer pathway, where an exponential function with a slower (smaller) kinetic rate is assigned with a smaller initial value of that exponential function. I this sense, the kinetic pattern of the dual-exponential function may need some attentions. According to Eq. (42), the two exponential components have the ratio of the initial values identical to the ratio of the kinetic rates. If a kinetic decay of monotonic change does not fit to a single exponential function, the next easiest fit will be a dual-exponential pattern that will produce two numbers for the kinetic rate or the inverse of the time constant, and two numbers for the initial value or the intensity of each exponential component. So if a kinetic decay pattern can be fitted with two exponential functions, one can identify if the kinetic pathway would be modeled by the system consisting of two first-order low-pass responses as shown in Figure 7, by comparing the ratio of the fitted intensities of the two exponential functions and the ratio of the kinetic rates of the two functions. That type of correlation between the intensity ratio and kinetic-rate ratio of a decay pattern that can fitted with dual-exponential functions was actually inferred [93].

The bolus response of the pathway hypothesized to have first-order low-pass transfer components is interesting. That response applies to a single exponential system, or the one with the largest kinetic rate. It should be noted that the response to a bolus input also represents the response to the falling phase when a step input is stopped, and that should indicate what may be expected at the falling edge of a pulse stress. The Eq. (38) for the response of a single first-order low-pass system to a bolus input implies that, a greater kinetic rate of photo-genesis by the metabolic engine not only causes the decay to be faster, but also makes the initial intensity to be stronger, at the condition of the same kinetic rate preceding the metabolic engine. This indication may be useful to understanding why the delayed UPE with shorter delay time or faster decay rate is generally stronger than those having longer delay time or slower decay rate. The kinetic time constants of delayed UPE in response to photic-stress can be a couple of orders of magnitude shorter than those of non-photic stress. That agrees with the observation that the initial intensity of delayed UPE in response to photo-stimulation can be a couple of orders of magnitude greater than those of non-photic stimulations. That faster response of the metabolic engine of photo-genesis to photic-stress than non-photic stimulation is intuitive. Regardless of how the photo-genesis occurs, the external stress must be passed and processed along the metabolic chain to the terminal process to modulate the sourcing of the photons emitted as delayed UPE. A photic-stress may be able to directly affect photo-sensitive receptors in the metabolic pathway, whereas the non-photic stress would require additional intermediate states that are either local or systematic, that will slow their effects down in terms of triggering the same type of responses in the terminal metabolic engine process of photo-genesis in comparison to what the photic-stress would stimulate. This phenomenon of stronger initial intensity associated with faster decay kinetics renders the possibility of acquiring more photons of delayed UPE by reducing the time-lag between the removal of the stress and the starting of the acquisition of delayed UPE if the stress can be turned off cleanly (i.e. no after-glow for photic sources). The shortest time-delay that has been used for delayed UPE acquisition is $8.5\mu s$, and the kinetic pattern associated with photo-stimulated delayed UPE generally reveal a one order of magnitude change of the intensity over one order of magnitude change of the time at the initial collection stage. Thus photon counting started at one-order of magnitude of time faster, i.e., $0.85\mu s$, may be accompanied with the initial photon count of one order of magnitude greater than what has been reported for photic-stimulation. Should the temporal delay between shutting off the photic-stimulation and starting the photon acquisition be further reduced, the initial photon-count of the delayed UPE may be further increased. It has been shown with the existing reports that the initial photon count of the delayed UPE in response to photic-stimulation can be as high as 5 orders of magnitude greater than the base-line level of spontaneous UPE [34], which is approximately 6 orders of magnitude weaker than the fluorescence signals excited by Cerenkov illumination [112]. It is thus may be possible to have a photon-count level of delayed UPE to reach the level of Cerenkov excited fluorescence, should the delayed UPE be acquired at a time-scale at least of 2 orders of magnitude faster than what has been shown now. This projection will certainly be incorrect, if the kinetics of the pre-$8.5\mu s$ duration of photic-stimulated delayed UPE does not follow the same first-order kinetics as appearing initially after the $8.5\mu s$ of starting the acquisition. If that happens, the initial stress-transfer response cannot be characterized by a first-order low-pass system having fixed kinetic rate, but rather it may indicate either a first-order system with varying kinetic rate or a second-order system that is over-damped. In either of these cases that would require fast time-correlated photon-counting, the shortening of the initial acquisition time will help identify more information of the stress-transfer pathway.

There are many assumptions implemented in this heuristic modeling work regarding the kinetic rates of the stress-transfer pathway that may seem overly simple and arbitrary. For example, the kinetic rate channeling the stress to the summating engine referring to a metabolic mechanism of phot-genesis is a constant. With this assumption of a constant rate for feeding the metabolic engine of photo-genesis, the intensity of source production as the output of the stress-transfer pathway will be proportional to the input, i.e. linearly dependent on the intensity of the stress. That does not agree with many delayed UEP patterns

in response to particularly photic-stimulation. It is appreciable that biological responses to external perturbations have limits. When the external perturbation exceeds a threshold of the biological response, the integrity of the physical or functional structure may be altered such that the response is no longer a quantitative change of the same entity but rather a complete mutation so the model applying to a quantitative variation of an integral entity of the same physical and functional manifestations will fail. The biological response of this kind of system to the input can be expected to be dependent non-linearly upon the intensity of the input, to have the kinetic rate saturate as the intensity of the external perturbation or stress approaches a threshold and that will cause the photo-genesis to saturate as the intensity approaches the threshold. The expectation of the saturation of the kinetic rate that transfers the stress to affect the metabolic engine of photo-genesis could possibly be associated with the multi-soliton coherent-state perspectives [42, 43, 61, 62] to interpret the non-linear dependence of the photo count in delayed UPE as a function of the intensity of the stress.

The bolus and step responses of the hypothesized stress-transfer pathway with a first-order low-pass behavior having a kinetic rate decreasing over time or equivalently the time constant increasing over time as shown in Fig. 12(B) and Fig. 13(B) are worth some attentions. The response of this system shall approach that of the single and pure exponential function when the kinetic rate barely changes over the duration of the acquisition. As the change of the kinetic rate increases, the response to both the bolus input and the step input become more and more like a hyperbolic pattern that starts from an initial peak in association with a bolus input or appears after a rapidly occurring peak in association with a step input. Such pattern of change is found in the oxidation current of superoxide anion radical ($O_2^{\blacksquare -}$) in response to wound that was investigated electrochemically [113]. Such behavior can be understood from the perspective of the frequency spectrum of the impulse response of the system. The kinetic rate of a first-order exponential function with the argument decaying over time is the low-pass cut-off frequency of the frequency spectrum of the impulse response. A faster kinetic rate means a higher cut-off frequency of the low-pass filtering, so an increased kinetic rate corresponds to increased passage of high-frequency components. The rising phase of the step stress carries the same frequency components as the bolus input, whereas the steady-state phase of the step stress gives the zero-frequency component. As the low-pass cut-off frequency is increased, more high-frequency components of the input will be passed so the output will resemble more of the response to a bolus input that has charged the system with an initial energy. Therefore the response to a step stress may be visually more informative than the response to a simple bolus input, in identifying stress-transfer responses that cannot be described by a simple exponential decay of fixed kinetic rate. Similar kinetic behavior can also be found with the over-damped case of the second-order band-pass responses. The over-damped case with second-order band-pass response is associated with two exponential functions having negative arguments. The kinetic rate of the two exponential functions that has the greater magnitude thus sets the low-pass cut-off frequency of the band-pass behavior, and so a large kinetic rate will pass more high-frequency components of the input that makes the response to a step input closer to that of the over-damped response to a bolus input. In fact, the use of frequency components of the delayed UPE to inform metabolic process using has been indicated [114]. More robust frequency-spectrum analysis of the delayed UPE can be expected when the delayed UPE can be acquired at signal-to-noise ratio much stronger than is available now, and that would require better understanding of the kinetics to facilitate instrumental approaches to enhance the detection efficiency and signal processing.

There are many limitations of this heuristic modeling frame-work that need to be addressed by future assessments. For example, the fast oscillatory response overlapping on a slowing changing global profile deviating from the base-line level may need to be accounted by combining a second-order underdamped pathway with a first order low-pass pathway or another second-order pathway that is over-damped. The kinetic rate of a rising phase may also differ from that of a falling phase of the stress, since one may associate with an agonistic or stimulatory pathway and the other may relate to an antagonistic or

inhibitory pathway. Should that be the case the level of the intensity change would differ between a rising phase and a falling phase of the same pulse stimulation [47]. That difference would however be proportional to the kinetic rate of the initial change that can be fitted with exponential decaying functions. In terms of the response of a stimulation that repeats, the stress-transferring output can be readily appreciated by comparing the scales of the period of the repeating stimulation and the temporal-response time of the pathway. For the cases of the pathway exhibiting first-order low-pass response, the longest time-constant will determine how the accumulative response will change. Apparently, if the period of the repeated stimulation is much longer (>5 times) of the longest time-constant of the system, the response to the repetitive stimulation will be seen as a simple repetition of the same single-stimulation output. If however the period of the repeated stimulation is comparable to the longest time-constant of the system, the response to the repetitive stimulation will have the response of the system to a single period of the input added to a previous period that has not set completely, and that will cause the upper and lower boundaries of the responses to change non-linearly, mostly following an slowly exponentially increasing pattern [47]. If the period of the repeated stimulation, or the duration of a step stress is even smaller than the shortest time-constant of the system, the response to the repetitive stimulation or a step stress may reveal near-linear changes of the photon count in response to a step or pulse stress like a heat shock [36] and linear increment of the photon count in response to repetitive stress [47].

With many limitations to address in future studies, this work has articulated that tissue scattering needs to be accounted for in identifying the causes of the temporal profiles of delayed UPE. That exploration has speculated the need of stress-transfer pathway that kinetically produces the photons at a temporal rate much slower than the life-time of photon propagation in tissue. The solutions developed for the temporal spread of the propagation of photons of UPE spectral relevancy in the spherical tissue domain will be specifically useful for future applications wherein the spatial origins of delayed UPE measured on the tissue surface need to be spatially resolved by way of spatially resolved detection sites on the tissue surface. The solution specific to optically homogeneous tissue conditions will also be useful as the model-basis for model-based analysis of delayed UPE from tissue domain that contains optical heterogeneities. The responses hypothesized for the limited cases of stress-transfer pathways may be useful to projecting stress modulation techniques to enhance the signal to noise ratio of UPE detection, for the potential of model-based spectroscopy or imaging to non-invasively explore the oxidative metabolism of organism.

7. Conclusion

Much remains to be understood for delayed ultraweak photon emission (UPE) from organism in association with oxidative burst following external perturbation, a phenomenon that has been experimented for over three decades. Delayed UPE often decays hyperbolically; yet, it is not uncommon to have delayed UPE that reveals first-order kinetic patterns characterized by single-exponential, double exponential, or multi-exponential changes. Some delayed UPEs also presented transient patterns that are characteristic of second-order responses. A soliton-based photon-storage model has addressed the hyperbolic decaying pattern of delayed UPE; however, there are questions outstanding regarding modeling other non-hyperbolic kinetics as well as the large range of temporal scales of delayed UPE that can vary from 8.5 microseconds to many hours. A soliton-based photon-storage model has addressed the common hyperbolic decaying pattern of delayed UPE; however, there are questions outstanding regarding modeling other non-hyperbolic kinetics as well as the large range of temporal scales of delayed UPE that can vary from 8.5 microseconds to many hours.This work proposes an alternative, heuristic model-framework for interpreting the various kinetic patterns of delayed UPE following stress. The delayed UPE is considered to be governed by two sequential phases: a stress-transfer phase that transforms the external stress to photo-genesis for emitting photons, and a photon-diffusion phase that transmits the photons emitted by the photo-genesis to the surface of organism for being detected as delayed UPE. Time-resolved

photon diffusion analysis reveals that any delayed UPE in organism with a delay time >100ns cannot be addressed by the inherent temporal spread that realistic tissue scattering will cause. A slow stress-transfer phase is thus required to explain the delay time-scales of delayed UPE at a minimum of 8.5μs as reported experimentally. The stress-transfer phase is hypothesized to carry the following types of responses: single or multiple 1st-order low-pass, single 2nd-order low-pass with various damping factors, and single 2nd-order band-pass with various damping factors. A single 1st–order low-pass response with a time-varying kinetic rate is also analyzed. The responses of these modeled pathways to bolus and step inputs demonstrate that a kinetic pattern other than the exact single-exponential one may have multiple causes. A slow stress-transfer pathway combined with the fast photon-diffusion process may be suitable to serve as the model-basis for interpreting the patterns of delayed UPE observed with various time-scales.

Acknowledgement
The author thanks his peer for encouraging this work, and Prof. Baohong Yuan for technical discussions.

REFERENCES

1. Cifra, M. and P. Pospisil, *Ultra-weak photon emission from biological samples: definition, mechanisms, properties, detection and applications.* J Photochem Photobiol B, 2014. **139**: p. 2-10.
2. Calcerrada, M. and C. Garcia-Ruiz, *Human Ultraweak Photon Emission: Key Analytical Aspects, Results and Future Trends - A Review.* Crit Rev Anal Chem, 2018: p. 1-14.
3. Oros, C.L. and F. Alves, *Leaf wound induced ultraweak photon emission is suppressed under anoxic stress: Observations of Spathiphyllum under aerobic and anaerobic conditions using novel in vivo methodology.* PLoS One, 2018. **13**(6): p. e0198962.
4. Popp, F.A., et al., *Biophoton emission. New evidence for coherence and DNA as source.* Cell Biophys, 1984. **6**(1): p. 33-52.
5. Quickenden, T.I. and S.S. Que Hee, *Weak luminescence from the yeast Saccharomyces cerevisiae and the existence of mitogenetic radiation.* Biochem Biophys Res Commun, 1974. **60**(2): p. 764-70.
6. Cadenas, E., A. Boveris, and B. Chance, *Low-level chemiluminescence of bovine heart submitochondrial particles.* Biochem J, 1980. **186**(3): p. 659-67.
7. Boveris, A., et al., *Spontaneous Chemiluminescence of Soybean Embryonic Axes during Imbibition.* Plant Physiol, 1984. **76**(2): p. 447-51.
8. Devaraj, B., M. Usa, and H. Inaba, *Biophotons: Ultraweak light emission from living systems.* Current Opinion in Solid State & Materials Science, 1997. **2**(2): p. 188-193.
9. Cohen, S. and F.A. Popp, *Biophoton emission of the human body.* J Photochem Photobiol B, 1997. **40**(2): p. 187-9.
10. Wang, J. and Y. Yu, *Relationship between ultra-weak bioluminescence and vigour or irradiation dose of irradiated wheat.* Luminescence, 2009. **24**(4): p. 209-12.
11. Havaux, M., C. Triantaphylides, and B. Genty, *Autoluminescence imaging: a non-invasive tool for mapping oxidative stress.* Trends Plant Sci, 2006. **11**(10): p. 480-4.
12. Moraes, T.A., et al., *Spontaneous ultra-weak light emissions from wheat seedlings are rhythmic and synchronized with the time profile of the local gravimetric tide.* Naturwissenschaften, 2012. **99**(6): p. 465-72.
13. Dotta, B.T., K.S. Saroka, and M.A. Persinger, *Increased photon emission from the head while imagining light in the dark is correlated with changes in electroencephalographic power: support for Bokkon's biophoton hypothesis.* Neurosci Lett, 2012. **513**(2): p. 151-4.
14. Wijk, R.V. and E.P. Wijk, *An introduction to human biophoton emission.* Forsch Komplementarmed Klass Naturheilkd, 2005. **12**(2): p. 77-83.
15. Glaser, A.K., et al., *Time-gated Cherenkov emission spectroscopy from linear accelerator irradiation of tissue phantoms.* Opt Lett, 2012. **37**(7): p. 1193-5.
16. Boveris, A., et al., *Organ chemiluminescence: noninvasive assay for oxidative radical reactions.* Proc Natl Acad Sci U S A, 1980. **77**(1): p. 347-51.
17. Cadenas, E., *Biological chemiluminescence.* Photochem Photobiol, 1984. **40**(6): p. 823-30.
18. Gallas, J.M. and M. Eisner, *Fluorescence of Melanin Dependence Upon Excitation Wavelength and Concentration.* Photochemistry and Photobiology, 1987. **45**(5): p. 595-600.
19. Kayatz, P., et al., *Oxidation causes melanin fluorescence.* Invest Ophthalmol Vis Sci, 2001. **42**(1): p. 241-6.
20. Kalaji, H.M., et al., *Experimental in vivo measurements of light emission in plants: a perspective dedicated to David Walker.* Photosynthesis Research, 2012. **114**(2): p. 69-96.
21. Fedorova, G.F., et al., *Peroxy-radical-mediated chemiluminescence: mechanistic diversity and fundamentals for antioxidant assay.* Arkivoc, 2007: p. 163-215.
22. Zhao, X., et al., *Spontaneous photon emission: A promising non-invasive diagnostic tool for breast cancer.* J Photochem Photobiol B, 2017. **166**: p. 232-238.

23. Kobayashi, M., T. Iwasa, and M. Tada, *Polychromatic spectral pattern analysis of ultra-weak photon emissions from a human body.* J Photochem Photobiol B, 2016. **159**: p. 186-90.
24. Wang, Z., et al., *Human high intelligence is involved in spectral redshift of biophotonic activities in the brain.* Proc Natl Acad Sci U S A, 2016. **113**(31): p. 8753-8.
25. Slawinski, J., *Luminescence research and its relation to ultraweak cell radiation.* Experientia, 1988. **44**(7): p. 559-71.
26. Iyozumi, H., K. Kato, and T. Makino, *Spectral shift of ultraweak photon emission from sweet potato during a defense response.* Photochem Photobiol, 2002. **75**(3): p. 322-5.
27. Nakamura, K. and M. Hiramatsu, *Ultra-weak photon emission from human hand: influence of temperature and oxygen concentration on emission.* J Photochem Photobiol B, 2005. **80**(2): p. 156-60.
28. Slawinski, J., et al., *Stress-induced photon emission from perturbed organisms.* Experientia, 1992. **48**(11-12): p. 1041-58.
29. Musumeci, F., A. Scordino, and A. Triglia, *Delayed luminescence from simple biological systems.* Riv Biol, 1997. **90**(1): p. 95-110.
30. Burgos, R.C.R., et al., *Cellular glutathione levels in HL-60 cells during respiratory burst are not correlated with ultra-weak photon emission.* J Photochem Photobiol B, 2017. **175**: p. 291-296.
31. Burgos, R.C.R., et al., *Ultra-weak photon emission as a dynamic tool for monitoring oxidative stress metabolism.* Sci Rep, 2017. **7**(1): p. 1229.
32. Rac, M., M. Sedlarova, and P. Pospisil, *The formation of electronically excited species in the human multiple myeloma cell suspension.* Sci Rep, 2015. **5**: p. 8882.
33. Niggli, H.J., et al., *Laser-ultraviolet-A-induced ultraweak photon emission in mammalian cells.* J Biomed Opt, 2005. **10**(2): p. 024006.
34. Baran, I., et al., *Mitochondrial respiratory complex I probed by delayed luminescence spectroscopy.* J Biomed Opt, 2013. **18**(12): p. 127006.
35. Scordino, A., et al., *Delayed luminescence to monitor programmed cell death induced by berberine on thyroid cancer cells.* J Biomed Opt, 2014. **19**(11): p. 117005.
36. Kobayashi, K., et al., *Biophoton emission induced by heat shock.* PLoS One, 2014. **9**(8): p. e105700.
37. Goraczko, W. and J. Slawinski, *Secondary Ultraweak Luminescence from Humic Acids Induced by gamma-Radiation.* Nonlinearity Biol Toxicol Med, 2004. **2**(3): p. 245-58.
38. Maccarrone, M., et al., *Kinetics of ultraweak light emission from human erythroleukemia K562 cells upon electroporation.* Biochim Biophys Acta, 1998. **1414**(1-2): p. 43-50.
39. Červinková, M.B.L.J.M.C.K. *Low frequency electromagnetic field effects on ultra-weak photon emission from yeast cells*. in *2016 ELEKTRO*. 2016.
40. Jain, A., et al., *Antioxidant efficacy on human skin in vivo investigated by UVA-induced chemiluminescence decay analysis via induced chemiluminescence of human skin.* Skin Pharmacol Physiol, 2010. **23**(5): p. 266-72.
41. Alvermann, M., et al., *Biological electric fields and rate equations for biophotons.* European Biophysics Journal with Biophysics Letters, 2015. **44**(3): p. 165-170.
42. Scordino, A., et al., *Delayed Luminescence From Collagen as Arising From Soliton and Small Polaron States.* International Journal of Quantum Chemistry, 2010. **110**(1): p. 221-229.
43. Popp, F.A. and K.H. Li, *Hyperbolic Relaxation as a Sufficient Condition of a Fully Coherent Ergodic Field.* International Journal of Theoretical Physics, 1993. **32**(9): p. 1573-1583.
44. Kataoka, Y., et al., *Activity-dependent neural tissue oxidation emits intrinsic ultraweak photons.* Biochemical and Biophysical Research Communications, 2001. **285**(4): p. 1007-1011.
45. Sauermann, G., et al., *Ultraweak photon emission of human skin in vivo: influence of topically applied antioxidants on human skin.* Methods Enzymol, 1999. **300**: p. 419-28.

46. Inaba, H., *Super-high sensitivity systems for detection and spectral analysis of ultraweak photon emission from biological cells and tissues.* Experientia, 1988. **44**(7): p. 550-9.
47. Footitt, S., et al., *Ultraweak Photon Emission from the Seed Coat in Response to Temperature and Humidity-A Potential Mechanism for Environmental Signal Transduction in the Soil Seed Bank.* Photochem Photobiol, 2016. **92**(5): p. 678-87.
48. al., E.G.B.e. *Design and implementation of a measurement system for ultra-weak bioluminescence detection from E. coli cultures applied to sanitary control*. in *2016 12th IEEE International Conference on Industry Applications (INDUSCON), Curitiba, 2016, pp. 1-4.* 2016.
49. Winkler, R., H. Guttenberger, and H. Klima, *Ultraweak and induced photon emission after wounding of plants.* Photochem Photobiol, 2009. **85**(4): p. 962-5.
50. Bajpai, R.P., P.K. Bajpai, and D. Roy, *Ultraweak photon emission in germinating seeds: a signal of biological order.* J Biolumin Chemilumin, 1991. **6**(4): p. 227-30.
51. Volodyaev, I. and L.V. Beloussov, *Revisiting the mitogenetic effect of ultra-weak photon emission.* Front Physiol, 2015. **6**: p. 241.
52. Shanei, A., et al., *Detection of Ultraweak Photon Emission (UPE) from Cells as a Tool for Pathological Studies.* J Biomed Phys Eng, 2017. **7**(4): p. 389-396.
53. Hossu, M., L. Ma, and W. Chen, *Nonlinear enhancement of spontaneous biophoton emission of sweet potato by silver nanoparticles.* J Photochem Photobiol B, 2010. **99**(1): p. 44-8.
54. Kageyama, C., et al., *Photon emissions from rice cells elicited by N-acetylchitooligosaccharide are generated through phospholipid signaling in close association with the production of reactive oxygen species.* Plant Physiol Biochem, 2006. **44**(11-12): p. 901-9.
55. Slawinska, D. and J. Slawinski, *Chemiluminescence of cereal products. I. Kinetics, activation energy and effects of solvents.* J Biolumin Chemilumin, 1997. **12**(5): p. 249-59.
56. Kimura, M., et al., *N-methyl-N'-nitro-N-nitrosoguanidine-induced light emission in Chinese hamster cell cultures: correlation with enhancement of chromosomal aberrations.* Mutat Res, 1992. **281**(3): p. 215-20.
57. Slawinska, D. and J. Slawinski, *Ultraweak photon emission in model reactions of the in vitro formation of eumelanins and pheomelanins.* Pigment Cell Res, 1987. **1**(3): p. 171-5.
58. Barsacchi, R., et al., *Correlation between hydroperoxide-induced chemiluminescence of the heart and its function.* Biochim Biophys Acta, 1983. **762**(2): p. 241-7.
59. Brizhik, L., et al., *The soliton mechanism of the delayed luminescence of biological systems.* Europhysics Letters, 2000. **52**(2): p. 238-244.
60. Popp, F.A. and Y. Yan, *Delayed luminescence of biological systems in terms of coherent states.* Physics Letters A, 2002. **293**(1-2): p. 93-97.
61. Brizhik, L., et al., *Nonlinear dependence of the delayed luminescence yield on the intensity of irradiation in the framework of a correlated soliton model.* Physical Review E, 2003. **67**(2).
62. Brizhik, L., et al., *Delayed luminescence of biological systems arising from correlated many-soliton states.* Physical Review E, 2001. **64**(3).
63. Chwirot, W.B., *Ultraweak photon emission and anther meiotic cycle in Larix europaea (experimental investigation of Nagl and Popp's electromagnetic model of differentiation).* Experientia, 1988. **44**(7): p. 594-9.
64. Musumeci, F., et al., *Spectral analysis of laser-induced ultraweak delayed luminescence in cultured normal and tumor human cells: temperature dependence.* J Photochem Photobiol B, 2005. **79**(2): p. 93-9.
65. Rosaria Grasso, F.P.C., Luigi Minafra, Valentina, G.R. Marchese, Lorenzo Manti, Francesco Musumeci, Agata, and Scordino. *Delayed luminescence in a multiparameter approach to evaluation and reduction of radiobiological risks*. in *Proc. SPIE 10413, Novel Biophotonics Techniques and Applications IV, 104130L (28 July 2017);* . 2017.

66. Sun, M., et al., *Delayed luminescence: an experimental protocol for Chinese herbal medicines.* Luminescence, 2016. **31**(6): p. 1220-8.
67. Grasso, R., et al., *Effects of Ion Irradiation on Seedlings Growth Monitored by Ultraweak Delayed Luminescence.* PLoS One, 2016. **11**(12): p. e0167998.
68. Wang, Y., et al., *Detecting Trace Amounts of Narcotics in Serum by Delayed Luminescence.* Ieee Photonics Journal, 2016. **8**(2).
69. Kim, H.W., et al., *Spontaneous photon emission and delayed luminescence of two types of human lung cancer tissues: adenocarcinoma and squamous cell carcinoma.* Cancer Lett, 2005. **229**(2): p. 283-9.
70. Chen, P., et al., *Spectral discrimination between normal and leukemic human sera using delayed luminescence.* Biomed Opt Express, 2012. **3**(8): p. 1787-92.
71. Gu, Q. and F.A. Popp, *Nonlinear response of biophoton emission to external perturbations.* Experientia, 1992. **48**(11-12): p. 1069-82.
72. Khabiri, F., et al., *Non-invasive monitoring of oxidative skin stress by ultraweak photon emission (UPE)-measurement. I: mechanisms of UPE of biological materials.* Skin Res Technol, 2008. **14**(1): p. 103-11.
73. Hagens, R., et al., *Non-invasive monitoring of oxidative skin stress by ultraweak photon emission measurement. II: biological validation on ultraviolet A-stressed skin.* Skin Res Technol, 2008. **14**(1): p. 112-20.
74. Bajpai, R.P. and P.K. Bajpai, *Light-induced biophotonic emission from plant tissues.* J Biolumin Chemilumin, 1992. **7**(3): p. 177-84.
75. Kataoka, Y., et al., *Activity-dependent neural tissue oxidation emits intrinsic ultraweak photons.* Biochem Biophys Res Commun, 2001. **285**(4): p. 1007-11.
76. Popp, F.A., et al., *Physical aspects of biophotons.* Experientia, 1988. **44**(7): p. 576-85.
77. Wang, C., et al., *Spontaneous and visible light-induced ultraweak photon emission from rat eyes.* Brain Res, 2011. **1369**: p. 1-9.
78. Collaboration, A., et al., *Measurement of the charge asymmetry in top quark pair production in pp collisions at [Formula: see text] using the ATLAS detector.* Eur Phys J C Part Fields, 2012. **72**(6): p. 2039.
79. Kruk, I., et al., *Chemiluminescence investigations of antioxidative activities of some antibiotics against superoxide anion radical.* Luminescence, 2011. **26**(6): p. 598-603.
80. Xie, Z. *Ultraweak bioluminescence of maize under NaCl stress*. in *Proc. SPIE 7513, 2009 International Conference on Optical Instruments and Technology: Optoelectronic Imaging and Process Technology, 75130W (24 November 2009)*. 2009.
81. Chi, G. *Using ultra-weak luminescence to evaluate NaCl stress resistance of maize varieties*. in *Proc. SPIE 7519, Eighth International Conference on Photonics and Imaging in Biology and Medicine (PIBM 2009), 75191V (28 October 2009)*. 2009.
82. Maccarrone, M., N. Rosato, and A. Finazzi Agro, *Lipoxygenase products induce ultraweak light emission from human erythroleukemia cells.* J Biolumin Chemilumin, 1997. **12**(6): p. 285-93.
83. Hossu, M., et al., *Enhancement of biophoton emission of prostate cancer cells by Ag nanoparticles.* Cancer Nanotechnol, 2013. **4**(1-3): p. 21-26.
84. Tada, S. and K. Okazaki, *A novel single-photon counting technique applied to highly sensitive measurement of [Ca2+]i transient in human aortic smooth muscle cells.* J Biomech Eng, 2006. **128**(5): p. 777-81.
85. Devaraj, B., et al., *Ultraweak light emission from rat liver nuclei.* Photochem Photobiol, 1991. **54**(2): p. 289-93.
86. Hideg, E., *On the Spontaneous Ultraweak Light-Emission of Plants.* Journal of Photochemistry and Photobiology B-Biology, 1993. **18**(2-3): p. 239-244.

87. Slawinski, J., *Biophotons from stressed and dying organisms: toxicological aspects.* Indian J Exp Biol, 2003. **41**(5): p. 483-93.
88. Vladimirov, Y.A., E.V. Proskurnina, and D.Y. Izmailov, *Chemiluminescence as a method for detection and study of free radicals in biological systems.* Bull Exp Biol Med, 2007. **144**(3): p. 390-6.
89. Prasad, A. and P. Pospisil, *Two-dimensional imaging of spontaneous ultra-weak photon emission from the human skin: role of reactive oxygen species.* J Biophotonics, 2011. **4**(11-12): p. 840-9.
90. Tang, R. and J. Dai, *Spatiotemporal imaging of glutamate-induced biophotonic activities and transmission in neural circuits.* PLoS One, 2014. **9**(1): p. e85643.
91. Yoshinaga, N., et al., *Ultraweak photon emission from herbivory-injured maize plants.* Naturwissenschaften, 2006. **93**(1): p. 38-41.
92. Prasad, A., A. Balukova, and P. Pospisil, *Triplet Excited Carbonyls and Singlet Oxygen Formation During Oxidative Radical Reaction in Skin.* Front Physiol, 2018. **9**: p. 1109.
93. Jaskowska, A., et al., *Kinetics studies of ultraweak luminescence induced by ascorbic acid in Characeae cells and their structures.* Luminescence, 2001. **16**(1): p. 51-6.
94. Tilbury, R.N., *The effect of stress factors on the spontaneous photon emission from microorganisms.* Experientia, 1992. **48**(11-12): p. 1030-41.
95. Aoshima, Y., K. Kato, and T. Makino, *Endogenous enzyme reactions closely related to photon emission in the plant defense response.* Indian J Exp Biol, 2003. **41**(5): p. 494-9.
96. WenLi Chen, Q.Z., Ling Li, Da Xing, Roeland Van Wijk, and YongHong Tang. *Comparing ultraweak bio-chemiluminescence emission in wounded green and etiolated soybean cotyledons*. in *Proc. SPIE 6088, Imaging, Manipulation, and Analysis of Biomolecules, Cells, and Tissues IV, 60881G (21 February 2006)*. 2006.
97. Voit, F., J. Schafer, and A. Kienle, *Light scattering by multiple spheres: comparison between Maxwell theory and radiative-transfer-theory calculations.* Opt Lett, 2009. **34**(17): p. 2593-5.
98. Ishimaru, A., *Diffusion of Light in Turbid Material.* Applied Optics, 1989. **28**(12): p. 2210-2215.
99. Arridge, S.R., M. Cope, and D.T. Delpy, *The Theoretical Basis for the Determination of Optical Pathlengths in Tissue - Temporal and Frequency-Analysis.* Physics in Medicine and Biology, 1992. **37**(7): p. 1531-1560.
100. Piao, D., et al., *On the geometry dependence of differential pathlength factor for near-infrared spectroscopy. I. Steady-state with homogeneous medium.* J Biomed Opt, 2015. **20**(10): p. 105005.
101. Piao, D.Q., *Photon diffusion in a homogeneous medium bounded externally or internally by an infinitely long circular cylindrical applicator. VI. Time-domain analysis.* Journal of the Optical Society of America a-Optics Image Science and Vision, 2014. **31**(10): p. 2232-2243.
102. Haskell, R.C., et al., *Boundary conditions for the diffusion equation in radiative transfer.* J Opt Soc Am A Opt Image Sci Vis, 1994. **11**(10): p. 2727-41.
103. Jacques, S.L., *Optical properties of biological tissues: a review.* Phys Med Biol, 2013. **58**(11): p. R37-61.
104. Yang, Y., et al., *Optical scattering coefficient estimated by optical coherence tomography correlates with collagen content in ovarian tissue.* J Biomed Opt, 2011. **16**(9): p. 090504.
105. Rivlin-Etzion, M., et al., *Low-pass filter properties of basal ganglia cortical muscle loops in the normal and MPTP primate model of parkinsonism.* J Neurosci, 2008. **28**(3): p. 633-49.
106. Wlodarczyk, J. and B. Kierdaszuk, *Interpretation of fluorescence decays using a power-like model.* Biophys J, 2003. **85**(1): p. 589-98.
107. Whitehead, L., et al., *A simple function for the description of near-exponential decays: The stretched or compressed hyperbola.* American Journal of Physics, 2009. **77**(2): p. 173-179.
108. Jung, H.H., et al., *Year-long biophoton measurements: normalized frequency count analysis and seasonal dependency.* J Photochem Photobiol B, 2005. **78**(2): p. 149-54.

109. Ou-Yang, H., *The application of ultra-weak photon emission in dermatology.* J Photochem Photobiol B, 2014. **139**: p. 63-70.
110. Zhao, X., et al., *Ultra-weak photon emission of hands in aging prediction.* J Photochem Photobiol B, 2016. **162**: p. 529-534.
111. Cadenas, E., et al., *Partial spectral analysis of the hydroperoxide-induced chemiluminescence of the perfused lung.* FEBS Lett, 1980. **111**(2): p. 413-8.
112. Tanha, K., A.M. Pashazadeh, and B.W. Pogue, *Review of biomedical Cerenkov luminescence imaging applications.* Biomed Opt Express, 2015. **6**(8): p. 3053-65.
113. Prasad, A., et al., *Real-time monitoring of superoxide anion radical generation in response to wounding: electrochemical study*. PeerJ, 2017. **5**: p. e3050.
114. Beloussov, L.V.e.a., *Statistical and frequency-amplitude characteristics of ultraweak emissions of the Loach egges and embroys under the normal conditions and upon theie optical interactions. 2. Change in characteristics of ultraweak emissions upon optic interactions of groups of embryos of different ages.* Russian Journal of Development Biology, 2003. **34**(6): p. 379-388.